nature microbiology

Article

https://doi.org/10.1038/s41564-026-02261-2

Skin androgens regulate *Staphylococcus aureus* pathogenicity via quorum sensing

Received: 20 March 2025

Accepted: 5 January 2026

Published online: 27 February 2026

Check for updates

Maria Sindhura John[1], Mahendran Chinnappan[1], Camille I. Sturges[1], Methinee Artami[1], Mohini Bhattacharya[2], Rebecca A. Keogh[2], Jeffrey S. Kavanaugh[2], Shivani Jain[1], Hanna Gedamu[1], Jessica Komarovsky[1], Mauricio Velasquez[3], Tripti Sharma[4], Jeffrey G. McDonald[3,5], Alexander R. Horswill[2,6] & Tamia A. Harris-Tryon[1,7]

Skin cells secrete testosterone, with greater amounts secreted at the skin surface of males compared with females. Males are also more susceptible to skin infections than females. Here we report that mice engineered with testosterone-deficient skin are resistant to methicillin-resistant *Staphylococcus aureus* infections. Testosterone promoted the expression of *S. aureus* cytotoxic virulence factors by activating the accessory gene regulator (*agr*) quorum-sensing pathway in a concentration-dependent manner and independent of quorum-sensing-activating auto-inducing peptides. Mutational analysis revealed that a functional histidine kinase AgrC in *S. aureus* was required for testosterone to exert its effect, with in silico evidence indicating a direct interaction between testosterone and AgrC. An isomer of testosterone, enantiomer-testosterone, that blocked bacterial quorum sensing, inhibited *S. aureus*-induced cytotoxicity of human cells. These findings advance our understanding of how the skin regulates bacterial virulence and reveals a potential therapeutic strategy for the management of infections.

Males are more susceptible to skin and soft tissue infections than females, yet the mechanisms driving these differences are unclear[1–3]. One established distinction between males and females is androgen production, including testosterone and dihydrotestosterone (DHT), generated by the testes and the ovaries[4]. The skin also generates and secretes nanomolar concentrations of hormones, including testosterone, with our previous liquid chromatography–tandem mass spectrometry (LC–MS/MS) studies showing site-specific differences in the abundance and repertoire of hormones at the skin surface[5,6]. Skin-colonizing bacteria are exposed to these hormones, yet their impact on bacterial pathogenesis remains unclear.

The majority of skin infections are caused by the opportunistic pathogen *Staphylococcus aureus*[7]. While *Staphylococcus epidermidis* and *Staphylococcus hominis* are established resident skin commensals, *S. aureus* is typically restricted to the anterior nares of approximately a third of healthy individuals, with skin colonization and infection occurring infrequently[8,9]. To colonize the skin, *S. aureus* requires virulence factors that are dampened by coordinated regulatory networks that tune their expression depending on sensed environmental conditions[10,11]. The most characterized regulatory system in *S. aureus* is the accessory gene regulator (*agr*) quorum-sensing system[11] that controls the expression of toxins and adhesins required for skin colonization and dermal invasion[12,13]. *Staphylococcus* auto-activates *agr* signalling through the production of auto-inducing peptide (AIP) signals[11]. Strains that lack functional *agr* signalling or *agr*-regulated factors, such as the phenol

[1]Department of Dermatology, University of Texas Southwestern Medical Center, Dallas, TX, USA. [2]Department of Immunology and Microbiology, University of Colorado School of Medicine, Aurora, CO, USA. [3]Center for Human Nutrition, University of Texas Southwestern Medical Center, Dallas, TX, USA. [4]Childrens Research Institute, University of Texas Southwestern Medical Center, Dallas, TX, USA. [5]Department of Molecular Genetics, University of Texas Southwestern Medical Center, Dallas, TX, USA. [6]Department of Veterans Affairs, Eastern Colorado Healthcare System, Aurora, CO, USA. [7]Department of Immunology, University of Texas Southwestern Medical Center, Dallas, TX, USA. e-mail: tamia.harris-tryon@utsouthwestern.edu

soluble modulin (PSM) peptides, show impaired skin infection[12,13]. Host and bacterially derived small molecules that inhibit *agr* have been described[14–16]. However, the skin cues that promote *S. aureus* pathogenesis at the skin surface remain incompletely understood. Increased understanding is critical to address the rising antibiotic resistance and lethality of methicillin-resistant *S. aureus* (MRSA)[17,18].

Here we investigated whether testosterone promotes *S. aureus* infection and found that mice engineered to secrete reduced levels of testosterone and DHT were resistant to MRSA infection. Further, testosterone and DHT activate MRSA and methicillin-sensitive *S. aureus* strains through stimulation of the *agr* quorum-sensing system. Using isogenic *agr* mutants and bioluminescent reporters, we found that testosterone is sufficient to activate quorum sensing, independent of the bacterially derived AIP. In addition, activation requires both the *agr* membrane histidine kinase receptor AgrC and the transcription factor AgrA. In silico modelling identified a testosterone binding site on AgrC distinct from the AIP binding site[19]. We further identified a stereoisomer of testosterone, enantiomer-testosterone (*ent*-T), as an inhibitor of *agr* signalling and *S. aureus*-mediated cytotoxicity. Together, these findings establish androgens as essential host signals for *S. aureus* skin infection and identify *ent*-T as a therapeutic candidate for the treatment of skin infections.

Results

Androgen secretion at the skin surface is required for *S. aureus* skin infection

Higher serum androgen production is associated with *S. aureus* colonization and infection[3,20]. However, there is limited understanding of androgen dynamics at the skin surface. Using LC–MS/MS, we quantified testosterone secretion from human skin through daily sebum sampling over 6 days in age-matched male and female participants without skin disease. Human skin consistently secreted between 5 nM and 10 nM testosterone with stable levels across days (Fig. 1a). In keeping with our previous study[5,6] of a larger cohort, the male participant secreted greater amounts of testosterone compared with the female subject (Fig. 1a,b). These findings demonstrate stable, sex-dependent secretion of nanomolar amounts of testosterone at the skin surface[5,6].

In addition to increased *S. aureus* in men versus women, *S. aureus* induces greater necrosis in male murine skin infections compared with female mice[2,3]. To confirm these findings, we epicutaneously infected male and female age-matched C57BL/6 mice with a bioluminescent strain of MRSA SAP430 (MRSA::*lux*). The MRSA::*lux* strain generates luminescence in direct proportion to the number of colony forming units (CFUs) present at the skin surface[21]. We observed increased infection severity in male mice compared with female mice (Fig. 1c and Extended Data Fig. 1). Male mice showed greater MRSA-induced bioluminescence imaging (BLI) and worse disease scores compared with female mice (Fig. 1c and Extended Data Fig. 1a,b). They also showed greater skin barrier damage (Extended Data Fig. 1c). In keeping with our human studies (Fig. 1a)[5], male mice secreted higher levels of the androgens testosterone and DHT at the skin surface compared with female mice (Extended Data Fig. 1d,e), again linking higher androgen secretion with increased infection severity.

To directly test the role of skin-derived androgens, we generated mice lacking epithelial expression of the steroidogenic enzyme 3β-hydroxysteroid dehydrogenase 6 (HSD3B6) (Fig. 1d)[22–24], a mouse orthologue of human *HSD3B1* (Extended Data Fig. 2a–d)[24]. *Hsd3b6*$^{\Delta skin}$ (*K14-Cre*$^{+/-}$; *Hsd3b6*$^{fl/fl}$) mice had the same amounts of serum hormones and weights compared with controls (Extended Data Fig. 2e,h). *Hsd3b6*$^{\Delta skin}$ mice also showed no differences in skin barrier function or histology compared with controls (Extended Data Fig. 2f,g). However, *Hsd3b6*$^{\Delta skin}$ mice secreted lower levels of testosterone, progesterone and DHT at the skin surface compared with *Hsd3b6*$^{fl/fl}$ mice (Fig. 1e,f and Extended Data Fig. 2i).

Next, we assessed the susceptibility of *Hsd3b6*$^{\Delta skin}$ mice to skin infection. Across 4 days of epicutaneous infection with MRSA::*lux*, the *Hsd3b6*$^{\Delta skin}$ mice showed reduced bioluminescence, lower diseases scores, less skin barrier damage and reduced epidermal thickness, suggesting that *Hsd3b6*$^{\Delta skin}$ mice are more resistant to skin infection compared with controls (Fig. 1g–i and Extended Data Fig. 3a). Complementing these findings in male mice, bacterially induced bioluminescence of female *Hsd3b6*$^{\Delta skin}$ mice infected with MRSA::*lux* were augmented by topical testosterone (Fig. 1j and Extended Data Fig. 3b,c). Topical testosterone also increased disease scoring, skin barrier disruption and epidermal thickness (Fig. 1k,l and Extended Data Fig. 3b). Reduction of skin-secreted hormones also minimized sex-dependent differences in infection between male and female mice (Fig. 1g,j, open circles and open squares). Thus, reduced secretion of testosterone, DHT and progesterone protected the skin from infection, and treatment with testosterone was sufficient to promote infection.

Testosterone and DHT activate *agr* quorum sensing and promote *S. aureus* pathogenesis

Next, to determine the direct impact of testosterone on the bacterial transcriptome, we sequenced RNA from a methicillin-sensitive strain of *S. aureus* (HG003 strain) treated with 10 nM of testosterone compared with vehicle treated control. Interestingly, testosterone had a narrow impact on the transcriptome of *S. aureus*, with increases in the expression of *agrB*, *agrD*, *agrC*, *agrA*, *psmα*, *psmβ* and *RNAIII* (Fig. 2a and Extended Data Fig. 4a–c), all of which were in the *agr* quorum-sensing pathway (Fig. 2b)[11,25]. Transcripts for the haemolysins *hlgB* and *hlgC*, which lyse human red blood cells (RBCs), were also more abundant

Fig. 1 | *Hsd3b6*$^{\Delta skin}$ mice with reduced androgen production in skin are resistant to *S. aureus* skin infection. a, Testosterone from site-matched skin secretions was quantified by LC–MS/MS in a man ($n = 1$) and woman ($n = 1$) without skin disease over 6 days. Data are presented as mean ± s.e.m. (error bars), with shaded areas representing the 95% confidence interval. *$P < 0.05$ by two-way ANOVA. **b**, Schematic showing sexual dimorphism of testosterone secretion in male and female back skin[5]. **c**, Bioluminescent MRSA SAP430 (MRSA::*lux*) epicutaneous skin infection in male and female ($n = 5$) C57BL/6 wild-type mice (1×10^6 CFU, 4 days). Bioluminescence quantified over time. Means ± s.e.m. (error bars) are plotted. *$P < 0.05$ by two-way ANOVA. **d**, Schematic of HSD3B6/1 enzyme-mediated conversion of pregnenolone to testosterone and DHT. *Hsd3b6*$^{\Delta skin}$ mice lack HSD3B6 enzyme function in the skin. **e**,**f**, Testosterone (**e**) and DHT (**f**) quantified from the skin secretions of male and female *Hsd3b6*$^{fl/fl}$ ($n = 11$) and *Hsd3b6*$^{\Delta skin}$ ($n = 8$) mice (7 weeks) by hormone immunoassay. Means ± s.e.m. (error bars) are plotted. **$P < 0.01$, ****$P < 0.0001$ by 2-way ANOVA (2-sided). **g**–**i**, Male *Hsd3b6*$^{fl/fl}$ ($n = 10$) and *Hsd3b6*$^{\Delta skin}$ ($n = 5$) mice epicutaneously infected with bioluminescent MRSA SAP430 (MRSA::*lux*, 1×10^6 CFU, 4 days). **g**, Left, bioluminescence quantified over time. Right, representative image of bioluminescence on day 1. Means ± s.e.m. (error bars) are plotted. *$P < 0.05$ by 2-way ANOVA. **h**, Left, disease score quantified on day 4. Right, representative image of skin inflammation on day 4. Means ± s.e.m. (error bars) are plotted. *$P < 0.05$, by 2-sided Mann–Whitney *U*-test. **i**, Transepidermal water loss (TEWL) quantified by Vapometer on day 0 and day 4. Means ± s.e.m. (error bars) are plotted. ****$P < 0.0001$ by 2-way ANOVA (two-sided). **j**–**l**, Female *Hsd3b6*$^{\Delta skin}$ mice were epicutaneously infected with bioluminescent MRSA SAP430 (MRSA::*lux*, 1×10^6 CFU, 4 days) with or without testosterone (vehicle $n = 3$; testosterone $n = 4$). **j**, Left, bioluminescence quantified over time. Right, representative images of bioluminescence on day 1. Means ± s.e.m. (error bars) are plotted. $P = 0.052$ by 2-way ANOVA. **k**, Left, disease score was quantified on day 4. Right, representative image of skin inflammation on day 4. $P = 0.057$ by 2-sided Mann–Whitney *U*-test. **l**, Transepidermal water loss was quantified by Vapometer on day 0 and day 4. Means ± s.e.m. (error bars) are plotted. ****$P < 0.0001$ by 2-way ANOVA (2-sided). See Extended Data Figs. 1–3. Illustrations created in BioRender: **b**, Harris, T. https://biorender.com/rpfp2in (2025); **d**, Harris, T. https://biorender.com/5iw1tsh (2025).

https://doi.org/10.1038/s41564-026-02261-2

in *S. aureus* treated with 10 nM of testosterone compared with controls (Extended Data Fig. 4a). Conversely, genes whose expression is repressed upon *agr* activation, including *coa*, *rot* and *spa*, were less abundant in testosterone-treated *S. aureus* (Extended Data Fig. 4a). In contrast, pregnenolone, a hormone with a similar carbon count to testosterone, had no discernible impact on the HG003 transcriptome (Extended Data Fig. 4d). Notably, treatment with testosterone or DHT did not alter *S. aureus* HG003 growth in culture (Extended Data Fig. 5a). Taken together, these findings suggested that testosterone stimulated *agr* quorum sensing in the HG003 strain of *S. aureus*.

Activation of *agr* quorum sensing in *S. aureus* occurs through the stimulation of the P2, P3 and PSM promoters that regulate the production of AIP-I synthesis and the PSM peptides (Fig. 2b)[11]. Therefore, to test the influence of sex steroids on *agr* signalling, we created P3 promoter

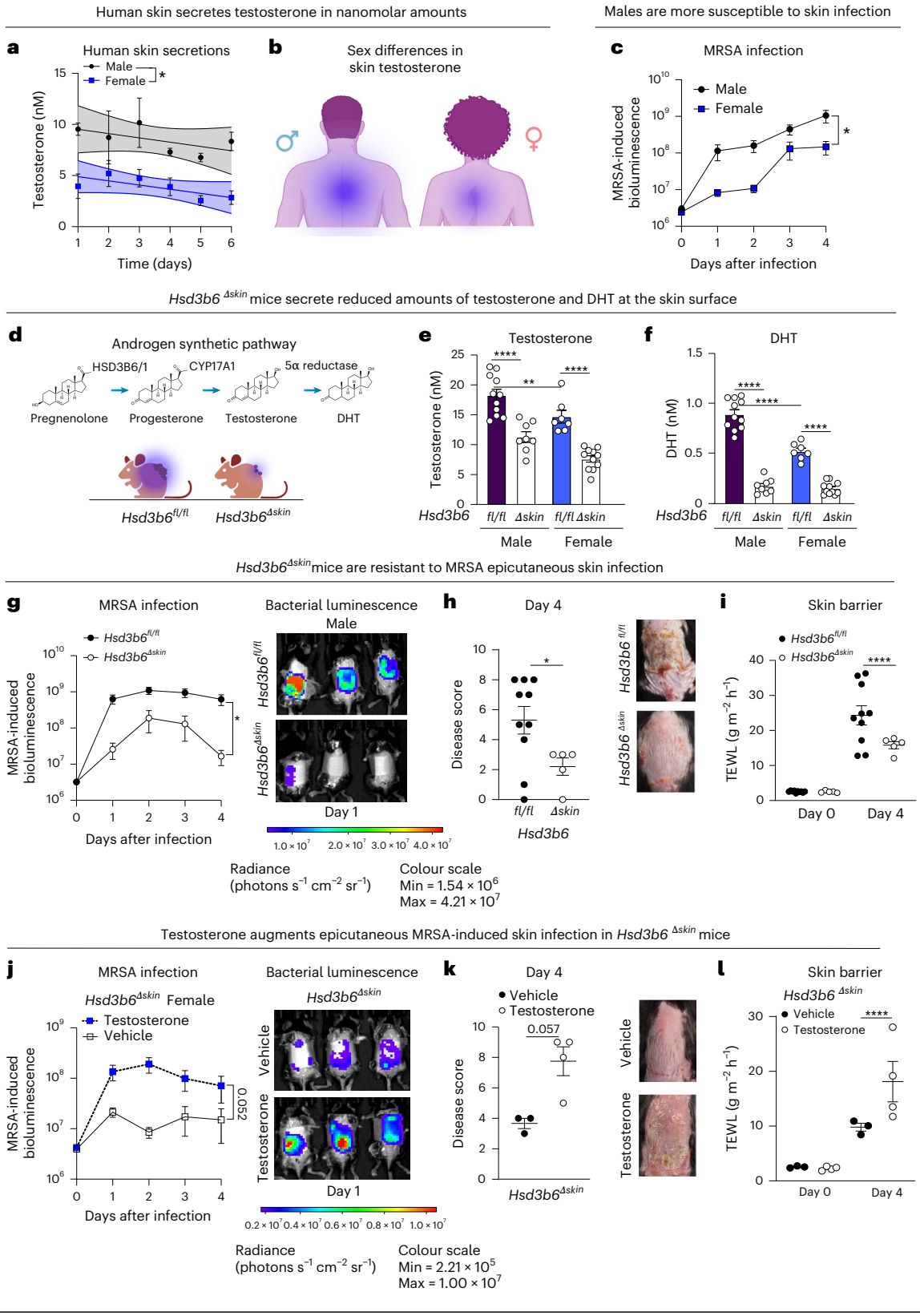

https://doi.org/10.1038/s41564-026-02261-2

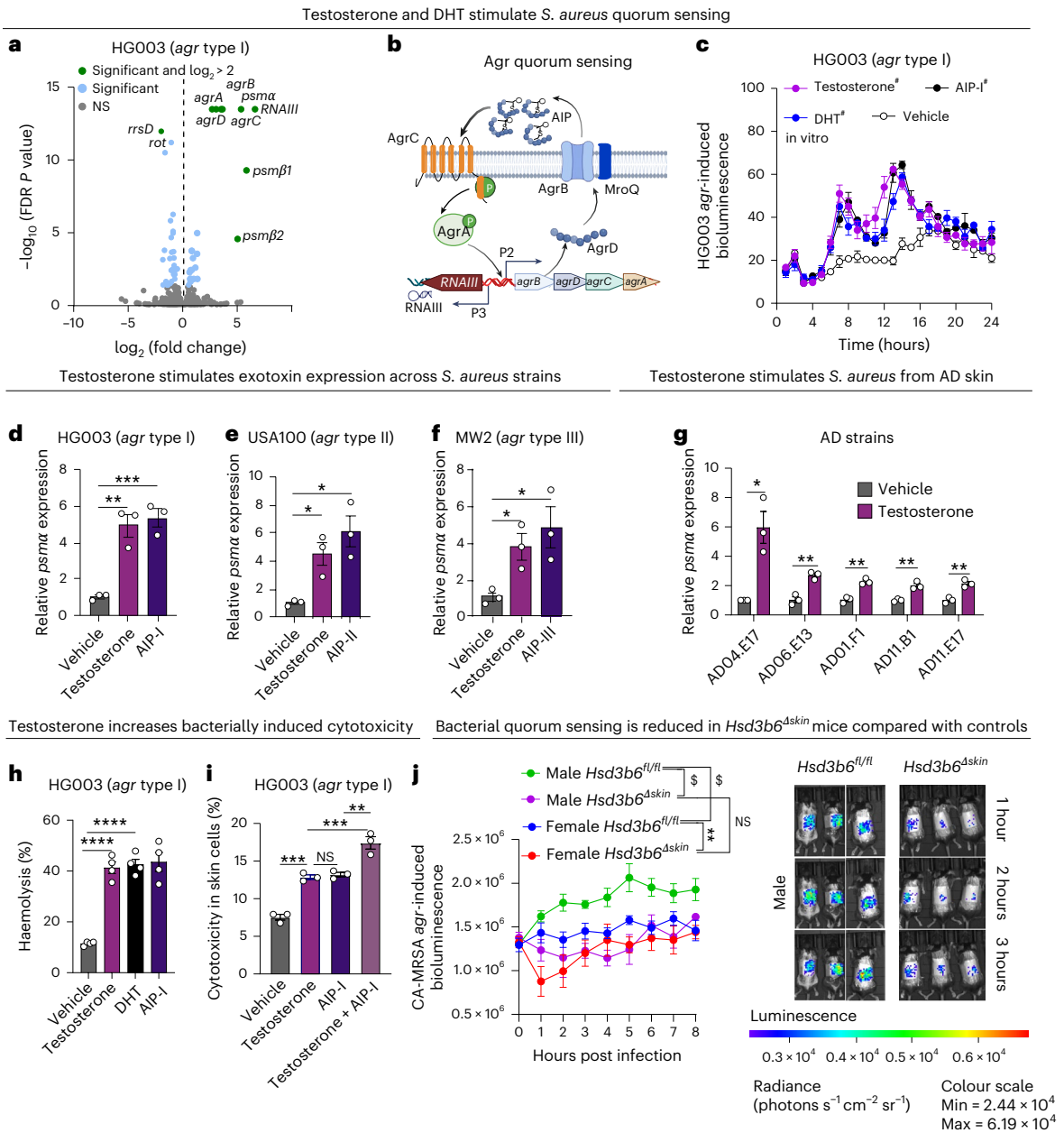

Fig. 2 | Testosterone and DHT stimulate *agr* quorum sensing and drive *S. aureus* pathogenesis. a, The *S. aureus* HG003 strain was treated with 10 nM testosterone or vehicle to early-log phase (OD_{600} = 0.4). Volcano plot showing genes with >4-fold expression change (green) by RNA sequencing. **b**, Schematic of *S. aureus agr* quorum-sensing system. **c**, *agr*-induced bioluminescence of HG003*agr*-P3::*lux* quorum-sensing reporter in vivo treated with 10 nM testosterone, DHT, AIP-I or vehicle ($n = 3$). Means ± s.e.m. (error bars) are plotted. $^{\#}P < 0.0001$ by 2-way ANOVA compared with vehicle. **d**, Quantitative real-time PCR (qRT-PCR) of *S. aureus* HG003 (type-I strain) treated with 10 nM testosterone, AIP-I or vehicle ($n = 3$) until mid-exponential growth (OD_{600} = 0.6). Gene expression is normalized to *gyrA*. Means ± s.e.m. (error bars) are plotted. $^{**}P < 0.01$, $^{***}P < 0.001$ by unpaired 2-tailed Student's *t*-test. **e**,**f**, qRT-PCR of MRSA type-II (USA100) (**e**) and MRSA type-III (MW2) (**f**) strains cultured to mid-log phase, treated with 10 nM testosterone, AIP-II or AIP-III ($n = 3$). *psmα* expression is normalized to *gyrA*. Means ± s.e.m. (error bars) are plotted. $^{*}P < 0.05$ by unpaired 2-tailed Student's *t*-test. **g**, qRT-PCR for *psmα* in *S. aureus* isolates from patients with AD[30] treated with 10 nM testosterone or vehicle ($n = 3$) to mid-exponential growth. Means ± s.e.m. (error bars) are plotted. $^{*}P < 0.05$, $^{**}P < 0.01$ by unpaired 2-tailed Student's *t*-test. **h**, Percentage of *S. aureus*-induced RBC haemolysis with and without 10 nM testosterone, DHT or AIP-I ($n = 4$ human donors, 2 men and 2 women). Means ± s.e.m. (error bars) are plotted. $^{****}P < 0.0001$, by 1-way ANOVA. **i**, Percentage of *S. aureus*-induced skin cell cytotoxicity with and without 10 nM testosterone, AIP-I or AIP-I and testosterone ($n = 3$). Means ± s.e.m. (error bars) are plotted. $^{**}P < 0.01$, $^{***}P < 0.001$ by 1-way ANOVA. **j**, *agr*-induced bioluminescence in vivo. Left, epicutaneous infection of male and female *Hsd3b6*$^{fl/fl}$ ($n = 7$ males and $n = 5$ females) and *Hsd3b6*$^{\Delta skin}$ mice ($n = 6$ males and $n = 5$ females) with bioluminescent CA-MRSA-*agr*-P3::*lux* with *agr*-induced bioluminescence quantified over time. Right, representative bioluminescence images. $^{\$}P < 0.0001$, $^{**}P < 0.01$ and non-significant (NS) by 2-way ANOVA with comparisons. Aggregate of two experiments. Means ± s.e.m. (error bars) are plotted. See Extended Data Figs. 4–6. Panel **b** created in BioRender; Harris, T. https://biorender.com/wd041bk (2025).

fusions of a *S. aureus* strain (HG003*agr*-P3::*lux*) that generate bioluminescence in proportion to the activation of quorum sensing[26]. Both testosterone and DHT activated the *agr*-P3 promoter, with similar kinetics to the established ligand AIP-I (Fig. 2c). However, oestradiol and progesterone had no impact on *agr* activation (Extended Data Fig. 5b). To confirm the effect of testosterone on *S. aureus*, we quantified the transcription of the read-outs of *agr*, *psmα*, *agrA* and *RNAIII*, and demonstrated that testosterone stimulates the expression of these

transcripts (Fig. 2d and Extended Data Fig. 5c). Thus, testosterone and DHT activate the transcription of the *agr* regulon in *S. aureus*, but oestradiol, pregnenolone and progesterone do not. These findings suggested that the lower infectivity of MRSA in the *Hsd3b6*$^{\Delta skin}$ mice compared with controls (Fig. 1g–l) was due to loss of testosterone and DHT at the skin surface, rather than reductions of progesterone (Extended Data Fig. 2i).

Every staphylococcal isolate contains a single copy of the *agr* system, and each species of *S. aureus* produces different types of AIP signal through variation in the *agrBDCA* operon[11]. There are four types of AIP signal made by *S. aureus* and the HG003 strain falls into the *agr* type-I class. To test the generality of the effects of testosterone across *agr* types, we treated different *agr* types with testosterone, including USA100 (MRSA type II) and MW2 (MRSA type III)[11]. All strains showed increased expression of *psmα* and *RNAIII* in response to 10 nM of testosterone (Fig. 2e,f and Extended Data Fig. 5d–i). Testosterone also activated the *agr*-P3 promoter in MRSA type-II and MRSA type-III luminescent strains (Extended Data Fig. 5e,h), indicating that testosterone stimulates virulence and quorum sensing across *S. aureus* strains. Again, treatment with testosterone and DHT had no impact on the growth curves of these strains in culture. More than 90% of *S. aureus* strains are type I–III[27], suggesting that testosterone stimulates virulence across *S. aureus* strains with active *agr* systems. Given the association between *S. aureus* and the skin disease atopic dermatitis (AD)[28,29], we also tested an array of strains obtained from diseased skin[30]. Indeed, testosterone treatment increased the transcription of *psmα*, *RNAIII* and the cytoplasmic regulator *agrA* in bacterial strains obtained from AD skin (Fig. 2g and Extended Data Figs. 6a,b). Notably, the AD04.E17 strain of *S. aureus* showed a more robust response to testosterone than the other AD-associated strains tested, and the response was of a similar magnitude to AIP-II stimulation (Fig. 2d–f and Extended Data Fig. 6c). These findings suggest that testosterone stimulation correlates closely with AIP stimulation at the same dose and may reflect the baseline *agr* activity of the strain. In addition, testosterone stimulated the transcription of cytotoxic virulence factors stimulated by AIPs, including *luk*S-*PV*, *hla* and *hld* (Extended Data Fig. 6d–f), and increased bacterially induced cytotoxicity of human cells, including skin cell death, RBC haemolysis and neutrophil killing (Fig. 2h,i and Extended Data Fig. 6g). These effects were comparable to those of AIP-I (Fig. 2h,i).

Finally, we compared quorum-sensing activity in vivo using a bioluminescent quorum-sensing reporter of the hypervirulent community-associated USA300 MRSA (CA-MRSA-*agr*-P3::*lux*). Consistent with our previous in vivo data using the constitutive *lux* reporter (Fig. 1g–l), bacterial quorum signalling was lower in *Hsd3b6*$^{\Delta skin}$ mice infected with the quorum-sensing reporter strain compared with *Hsd-3b6*$^{fl/fl}$ controls (Fig. 2j and Extended Data Fig. 6h). *agr* activation in vivo was also greater in male mice compared with female mice (Fig. 2j). Taken together, these data show that androgens stimulate the *S. aureus* quorum-sensing system in vitro and in vivo and have the capacity to increase bacterial cytotoxicity.

Testosterone stimulates *S. aureus* pathogenesis independently of the bacterial AIP

The established activator of *agr* type-I quorum sensing in *S. aureus*, AIP-I, is generated by the transcription of a propeptide AgrD, which is then processed by the endopeptidases AgrB and MroQ (Fig. 2b)[25]. Thus, the biosynthesis mutant Δ*agrBD* strain of *S. aureus* (HG003), which cannot synthesize AIP-I, is unable to auto-stimulate the quorum-sensing system[16]. We hypothesized that testosterone would require AIP-I to activate quorum sensing. However, in the biosynthesis mutant strain of methicillin-sensitive *S. aureus* (HG003-Δ*agrBD*), testosterone retained the ability to activate quorum-sensing phenotypes, including increased damage to skin cells, RBCs and neutrophils (Fig. 3a,b and Extended Data Fig. 7e). These effects were dose dependent, with greater concentrations of testosterone increasing the transcription of *RNAIII*, *agrA*, *agrC* and *psmα* (Extended Data Fig. 7a). In addition, we generated a luminescent reporter (Δ*agrBD*::*lux)* and tested the impact of progesterone and oestradiol on *S. aureus*. As in the wild-type reporter HG003 *agr*-P3 strain (Extended Data Fig. 5b), neither progesterone nor oestradiol stimulated luminescence in Δ*agrBD*::*lux* (Extended Data Fig. 7c), and neither DHT nor testosterone influenced bacterial growth curves in the Δ*agrBD* strain (Extended Data Fig. 7b). However, DHT and testosterone were both able to stimulate bioluminescence in the absence of AIP-I (Extended Data Fig. 7c). As AIP and testosterone could act independently, we next tested the impact of both AIP and testosterone on *agr* signalling. Indeed, treatment of *S. aureus* with testosterone had the capacity to augment AIP-I signalling in a dose-dependent manner (Fig. 3d and Extended Data Fig. 7d), establishing that testosterone may synergize with AIP signals to regulate pathogenesis.

Although AIP-I auto-stimulates quorum sensing in type I *S. aureus* strains, AIP-II and AIP-III, generated from type-II and type-III *S. aureus* strains respectively, inhibit quorum sensing in type-I strains (Extended Data Fig. 7f). Indeed, probiotics of strains that inhibit quorum sensing by generating inhibitory peptides are in development as *S. aureus* therapeutics[11,31]. To understand how skin-secreted testosterone might impact these inhibitory signals from other bacteria, we tested how testosterone competes with inhibitory signals derived from strains that generate non-cognate AIPs. Interestingly, when we exposed a type-I *S. aureus* strain to equal low nanomolar concentrations of AIP-II and testosterone, quorum sensing was inhibited, demonstrating that testosterone was unable to overcome inhibitory signals at the same concentration (Fig. 3e and Extended Data Fig. 7g). However, at higher concentrations, testosterone stimulated quorum sensing and overcame the inhibitory AIP-II signal (Fig. 3e and Extended Data Fig. 7g). Similar dynamics were observed with AIP-III (Fig. 3f and Extended Data Fig. 7h). These findings suggest that skin testosterone participates in the established crosstalk between competing microorganisms at the skin surface and can overcome inhibitory signals from other bacteria in a dose-dependent manner.

Lastly, we used the mutant Δ*agrBD*::*lux* strain to examine how loss of the AIP-I signal would impact bacterial infections in vivo. Interestingly, the mutant Δ*agrBD*::*lux* strain was able to infect the *Hsd3b6*$^{fl/fl}$ mice with similar kinetics to the MRSA::*lux* strain (black dots in Figs. 1g and 3g). In contrast, the *Hsd3b6*$^{\Delta skin}$ mice, with reduced androgen production on skin, showed reduced luminescence (Fig. 3g,h). The addition of testosterone or AIP-I on day 0 was able to partially rescue the intensity of infection in the *Hsd3b6*$^{\Delta skin}$ mice at day 1 post-inoculation (Fig. 3g). These findings show that skin-derived androgens are sufficient to facilitate *S. aureus* skin infection through activation of *agr* quorum sensing, even in the absence of AIPs.

Testosterone stimulation of *S. aureus* requires bacterial expression of the histidine kinase AgrC

AIPs stimulate the *agr* system through binding and activation of the AgrC histidine kinase[11,19]. Once activated, AgrC phosphorylates the response regulator AgrA that auto-induces transcription of the *agr* machinery (Fig. 2b)[11,32]. Given the specific impact of testosterone on the *agr* (Fig. 2a and Extended Data Fig. 4) and its ability to cooperate or compete with established ligands of AgrC (Fig. 3)[19], we tested if testosterone would require a complete AgrCA two-component system to regulate *S. aureus* virulence. We generated a constitutive bioluminescent reporter deficient in AgrC (Δ*agrC*::*lux*)[16]. In contrast to the biosynthetic Δ*agrBD*::*lux* mutant, the *ΔagrC*::*lux* mutant did not respond to testosterone in vitro (Fig. 4a). *S. aureus* required both AgrC and AgrA to respond to testosterone (Fig. 4b,c and Extended Data Fig. 7j–n). In Δ*agrC* mutants, testosterone failed to increase *psmα* or *RNAIII* expression and did not enhance haemolytic activity, neutrophil killing or skin cell cytotoxicity. Complementation of the Δ*agrC* mutant with AgrC in *trans* restored responsiveness to testosterone and AIP. In vivo, the loss of AgrC also decreased skin infections compared with infection

https://doi.org/10.1038/s41564-026-02261-2

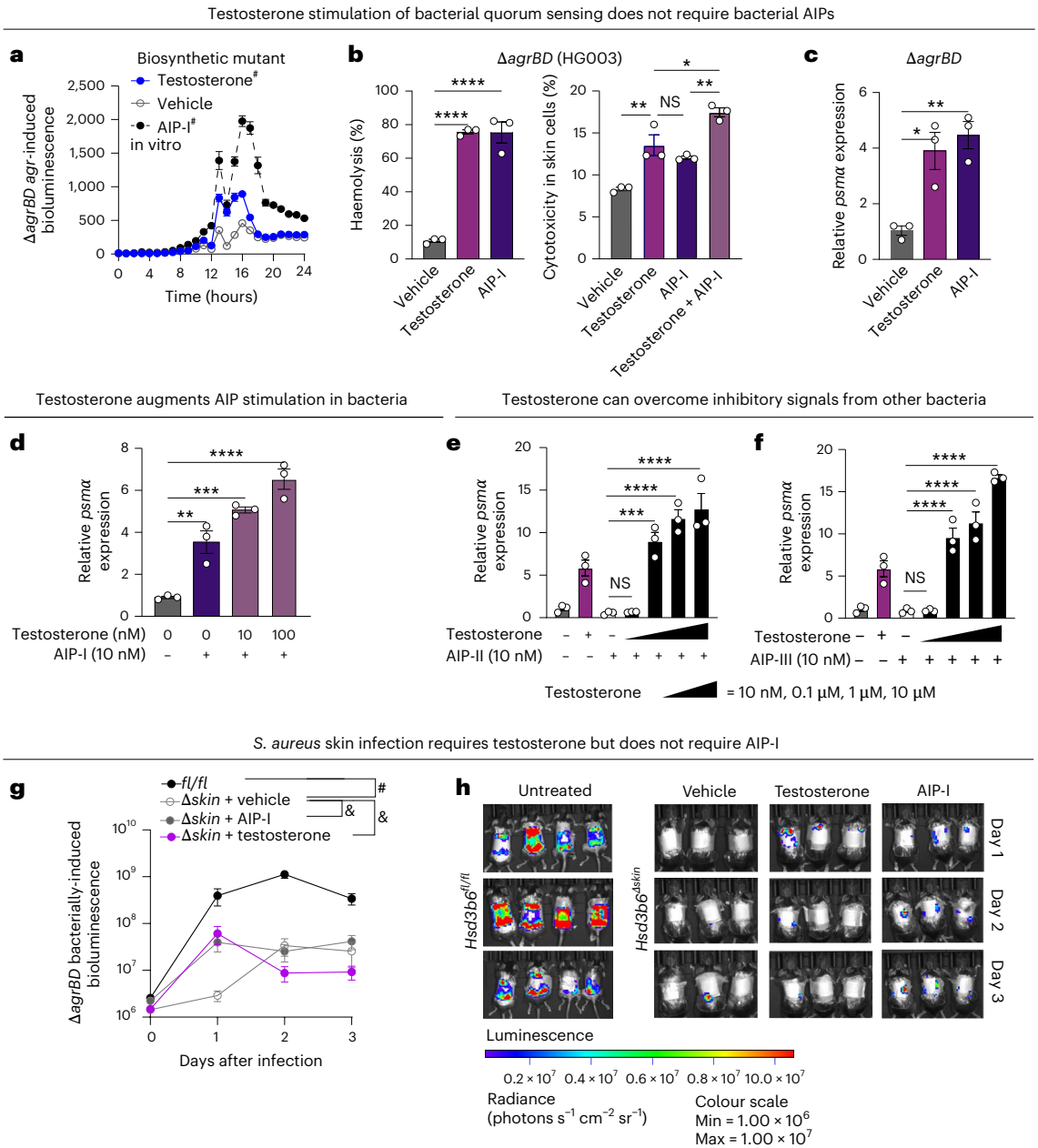

Fig. 3 | Testosterone stimulates *S. aureus* quorum sensing independently of the AIPs. a–**c**, *S. aureus* biosynthetic mutant (HG003-Δ*agrBD*) and its respective *agr*-P3 bioluminescent reporter strain (Δ$agrBD_{agr\text{-}P3}$::*lux*) were treated with 10 nM testosterone, AIP-I or untreated. **a**, *agr*-induced bioluminescence of *agr*-P3::*lux* was recorded every hour using a plate reader ($n = 12$). Statistics of testosterone and AIP-I compared with the vehicle. Means ± s.e.m. (error bars) are plotted. $^{\#}P < 0.0001$ by 2-way ANOVA compared with vehicle. **b**, Percentage of bacterially induced haemolysis and skin cell cytotoxicity ($n = 3$ replicates of RBCs from a single donor). **c**, qRT-PCR of *psmα* expression in the biosynthetic mutant strain treated with 10 nM testosterone, AIP-I and vehicle ($n = 3$), normalized to *gyrA* expression. **d**, qRT-PCR for *psmα* expression in the biosynthetic mutant strain treated with AIP-I and 10 nM or 100 nM of testosterone ($n = 3$). **e**,**f**, qRT-PCR for *psmα* expression in the biosynthetic mutant strain treated with AIP-II (**e**) or AIP-III (**f**) alone or in combination with increasing concentrations of testosterone (10 nM to 10 µM) ($n = 3$). **b**–**f**, Means ± s.e.m. (error bars) are plotted. $^{*}P < 0.05$, $^{**}P < 0.01$, $^{***}P < 0.001$, $^{****}P < 0.0001$ by 1-way ANOVA. **g**,**h**, Male *Hsd3b6*$^{fl/fl}$ ($n = 8$) and *Hsd3b6*$^{\Delta skin}$ ($n = 5$ per group) mice were epicutaneously infected with 1×10^6 CFU of the biosynthetic mutant strain constitutive reporter (Δ*agrBD*::*lux*) treated topically with testosterone, AIP-I or untreated, with bioluminescence quantified over time (**g**) and representative bioluminescence images (**h**). Results are an aggregate of two experiments. Means ± s.e.m. (error bars) are plotted. $^{\#}P < 0.01$ by 2-way ANOVA of *Hsd3b6*$^{fl/fl}$ compared with vehicle-treated *Hsd3b6*$^{\Delta skin}$ mice. $^{\&}P < 0.01$ by 2-sided Mann–Whitney *U*-test of vehicle compared with testosterone-treated *Hsd3b6*$^{\Delta skin}$ mice on day 1. See Extended Data Fig. 7a–h.

with intact AgrC (Fig. 4d). Similar to HG003 and Δ*agrBD*, testosterone treatment did not affect Δ*agrC* bacterial growth (Extended Data Fig. 7i). As expected, neither exogenous testosterone nor AIP-I were able to restore infection phenotypes in the *agrCA*-deficient strains (Fig. 4b,c,e and Extended Data Fig. 7j–m). These results show that *S. aureus* skin infection is influenced by both the skin secretion of androgens and a functioning AgrCA two-component system.

Finally, to gain further insight on interactions between AgrC and testosterone, we predicted the structure of the AgrC type-I dimer using AlphaFold 3 (AF3)[33,34] and docked testosterone and AIP-I on the AgrC sensory domain[35–37] (Fig. 4f). In silico analysis predicts testosterone binding to a hydrophobic cleft distinct from the established AIP binding site. A binding site distinct from the catalytic site and from the site of AIP-I binding is consistent with our data demonstrating

https://doi.org/10.1038/s41564-026-02261-2

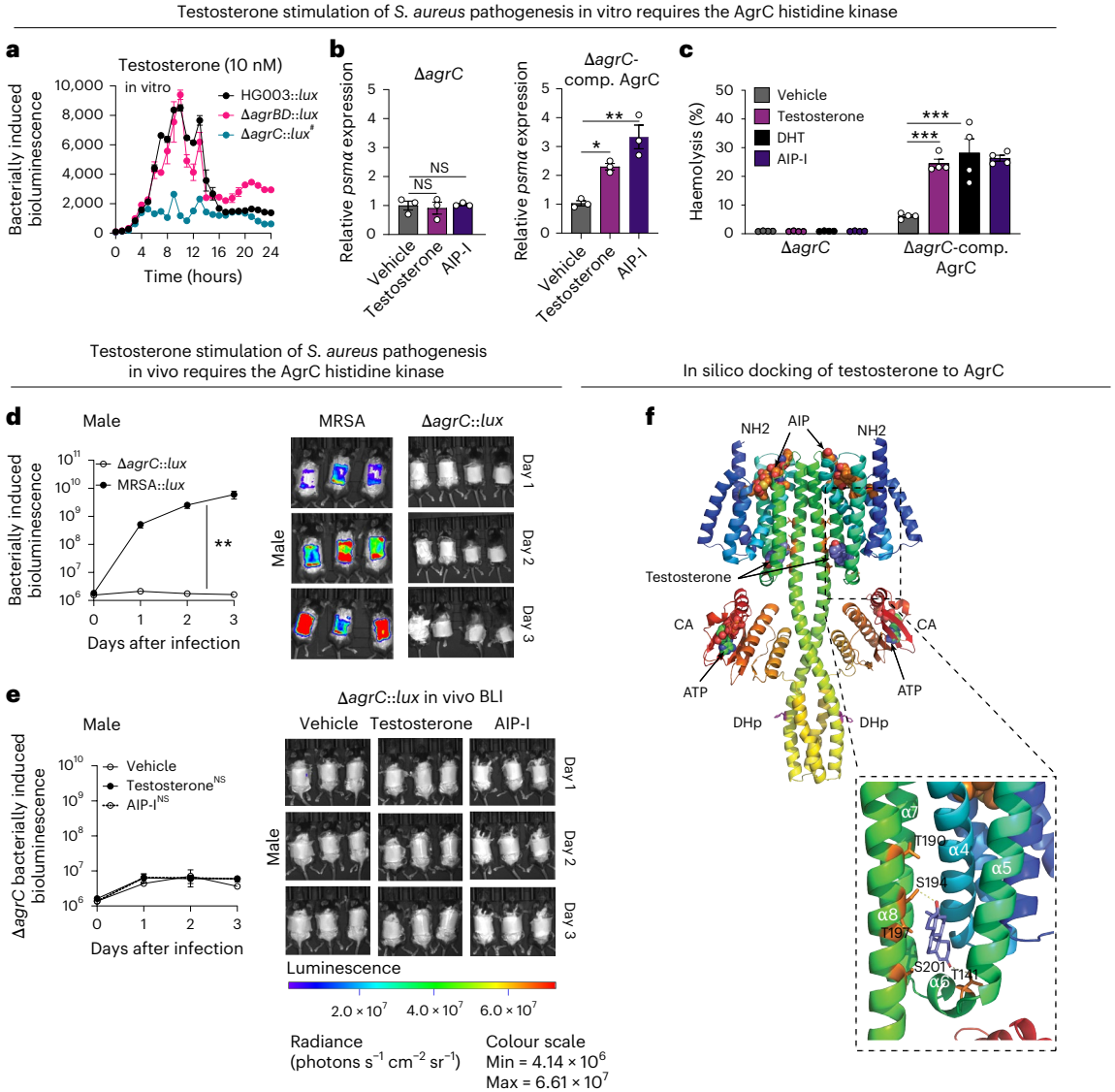

Fig. 4 | Testosterone stimulation of quorum sensing requires the histidine kinase AgrC. a, *S. aureus* wild-type (HG003::*lux*) and mutant constitutive bioluminescent reporter strains (Δ*agrBD*::*lux* and Δ*agrC*::*lux)* treated with 10 nM testosterone ($n = 3$). Bioluminescence is recorded every hour using a plate reader. Statistics of HG003 compared with Δ*agrC* treated with testosterone. Means ± s.e.m. (error bars) are plotted. $^{\#}P < 0.0001$ by 2-way ANOVA. **b**,**c**, Δ*agrC* mutant and Δ*agrC*-complemented strains (Δ*agrC*-comp. AgrC) treated with 10 nM testosterone, DHT, AIP-I or untreated ($n = 3$). Relative *psmα* expression (**b**) and percentage of bacterially induced haemolysis (**c**) ($n = 4$) technical replicates are shown; RBCs are from a single donor. Means ± s.e.m. (error bars) are plotted. $^{*}P < 0.05$, $^{**}P < 0.01$, $^{***}P < 0.001$, by 1-way ANOVA. **d**, Male wild-type mice ($n = 5$) were epicutaneously infected with bioluminescent MRSA SAP430 (MRSA::*lux*, 1×10^6 CFU) or AgrC-histidine-kinase-deficient (Δ*agrC*::*lux*) *S. aureus* ($n = 6$). An aggregate from two experiments is shown. Representative bioluminescence is shown. Means ± s.e.m. (error bars) are plotted. $^{**}P < 0.01$ by 2-way ANOVA. **e**, Male wild-type mice were infected with Δ*agrC*::*lux* (1×10^6 CFU, 3 days), treated with testosterone ($n = 5$), AIP-I ($n = 5$) or vehicle control ($n = 5$). Means ± s.e.m. (error bars) are plotted. NS by two-way ANOVA compared with vehicle control. **f**, The predicted dimeric structure of AgrC bound to AIP-I and testosterone shown as a rainbow-coloured ribbon (blue to red, amino to carboxy terminus), with the catalytic ATP-binding (CA) and dimerization/histidine phosphotransfer (DHp) domains. Testosterone, AIP-I and ATP are depicted as spheres (nitrogen, blue; oxygen, red; sulfur, yellow; phosphorus, orange; carbon, orange, purple and green for AIP-I, testosterone and ATP, respectively). The polar side chains of residues T141 (helix α6), T190, S194, T197 and S201 (helix α8) are shown. Enlarged insert: highest-affinity docking solution of testosterone is shown. See Extended Data Fig. 7i–n.

cooperative interactions between AIP-I and testosterone in type-I strains (Fig. 3d–f).

The enantiomer of testosterone inhibits MRSA pathogenesis

To further investigate the specificity of testosterone's interaction with the *agr* system, we tested the impact of a stereoisomer of testosterone, *ent*-T, on *S. aureus* pathogenesis. Enantiomer steroids have the same physiochemistry and impact on biological membranes, but can have distinct effects on receptors and signalling[38,39]. Similarly to other synthetic enantiomers, *ent*-T has a mirror image orientation at all six chiral centres of testosterone that leads to altered rotation of polarized light (Fig. 5a)[39,40]. In contrast to the other hormones tested with neutral effects on quorum sensing (Fig. 2c and Extended Data Fig. 5b), *ent*-T acted as an inhibitor of *agr* (Fig. 5 and Extended Data Fig. 8). *ent*-T decreased *S. aureus*-dependent RBC haemolysis and neutrophil killing (Fig. 5b,c). Further, *ent*-T decreased the expression of quorum-sensing-dependent virulence factors in MRSA type-II, MRSA type-III and AD strains of *S. aureus* (Fig. 5d–f, and Extended Data Fig. 8a). At higher concentrations, *ent*-T could also outcompete testosterone and turn off quorum sensing in vitro (Extended Data Fig. 8b). In keeping with their shared

https://doi.org/10.1038/s41564-026-02261-2

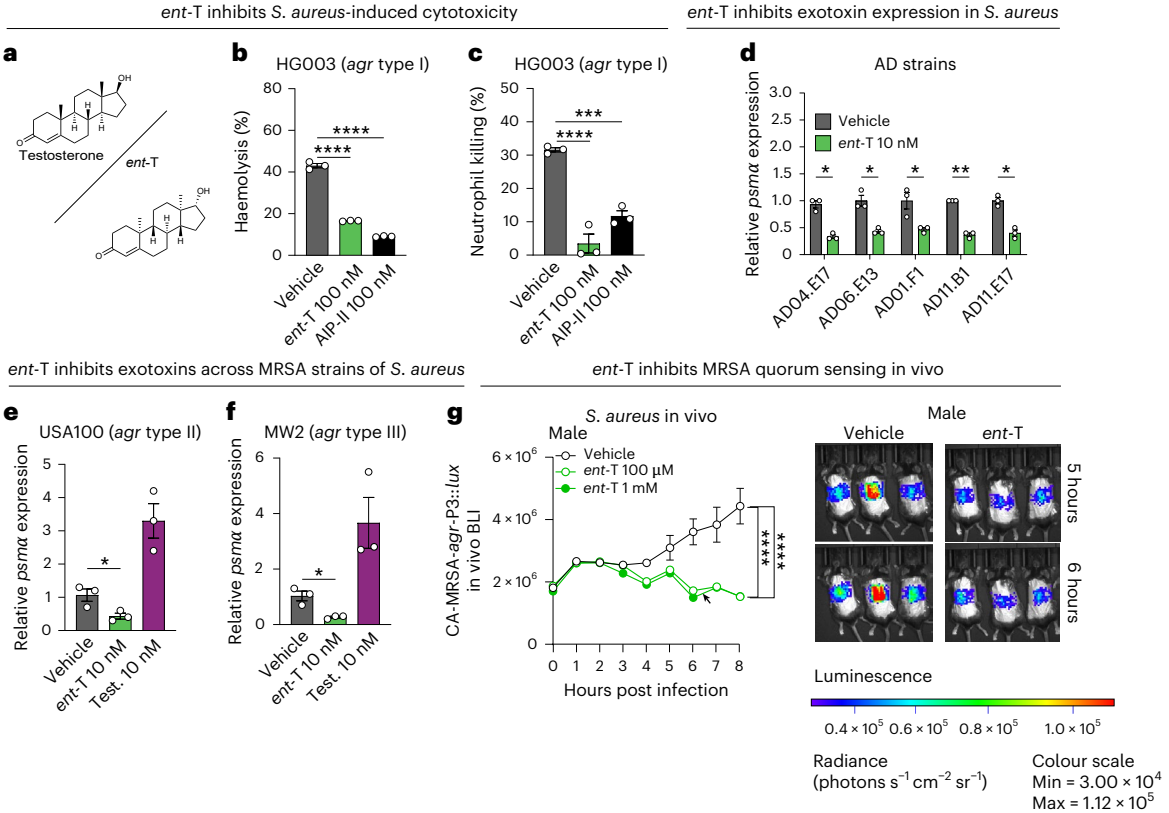

Fig. 5 | *ent*-T inhibits *S. aureus* quorum sensing and cell damage. a, Structure of testosterone and its stereoisomer *ent*-T. **b**,**c**, Wild-type *S. aureus* (HG003) treated with 100 nM of *ent*-T, AIP-II or untreated (vehicle). The percentage of bacterially induced haemolysis (**b**) and neutrophil killing (**c**) ($n = 3$ from single neutrophil and RBC donors) is shown. Means ± s.e.m. (error bars) are plotted. ***$P < 0.001$, ****$P < 0.0001$ by 1-way ANOVA. **d**–**f**, qRT-PCR for *psmα* expression in AD[30] strains ($n = 3$) (**d**), MRSA *agr* type II (**e**) and MRSA type III (**f**) *S. aureus* strains treated with 10 nM of testosterone or 10 nM of *ent*-T ($n = 3$). Relative expression of *psmα* is normalized to housekeeping gene *gyrA* expression. Means ± s.e.m. (error bars) are plotted. *$P < 0.05$, **$P < 0.01$ by paired 2-tailed Student's *t*-test (**d**); *$P < 0.05$ by unpaired 2-tailed Student's *t*-test (**e**,**f**). **g**, Male wild-type mice were epicutaneously infected with 1×10^6 CFU CA-MRSA-*agr*-P3 *S. aureus* quorum-sensing reporter treated with *ent*-T or vehicle (similar to in vivo analysis of Fig. 2j). Representative images (right) and bioluminescence quantified over time (left). Vehicle ($n = 5$), *ent*-T 1 mM ($n = 5$) or *ent*-T 100 µM ($n = 5$). Means ± s.e.m. (error bars) are plotted. ****$P < 0.0001$ of *ent*-T-treated groups compared with control by 2-way ANOVA. See Extended Data Fig. 8.

hydrophobicity properties, in silico analysis identified a high-affinity binding solution for *ent*-T bordered by residues T141, T197 and S201 of AgrC. Testosterone is predicted to bind to the same location; however, the orientation of its hydroxyl group is predicted to form hydrogen bonds with T190 and S194, which are not predicted for the chiral orientation of the *ent*-T hydroxyl groups (Extended Data Fig. 8c). Lastly, we tested how *ent*-T would impact *S. aureus agr* quorum sensing in vivo using the CA-MRSA-*agr*-P3::*lux*. Topical application of *ent*-T to mice skin infected with the CA-MRSA-*agr*-P3::*lux* reporter lowered quorum sensing in vivo in both male and female mice (Fig. 5g and Extended Data Fig. 8d–f). These data demonstrate that *ent*-T inhibits *S. aureus* cytotoxicity of human skin cells, RBCs and neutrophils by antagonizing *agr* quorum-sensing signalling[41].

Discussion

Here we have identified that the androgens testosterone and DHT regulate the pathogenesis of *S. aureus*, including lethal antibiotic-resistant MRSA strains (Fig. 1). Testosterone regulates *S. aureus* specifically through stimulation of a bacterial communication system called quorum sensing. Moreover, androgens can signal this system independently of the well-characterized, bacterially produced agonist of quorum sensing, AIP (Figs. 2 and 3). Further, in the absence of skin androgens, bacterial infection is diminished and sex-dependent differences in infection are markedly reduced (Figs. 1g,j). Our data also show that testosterone signalling of quorum sensing requires the expression of the *S. aureus* histidine kinase receptor AgrC and the response regulator AgrA (Fig. 4 and Extended Data Fig. 7a–d). In silico analysis supports testosterone binding directly to the transmembrane protein AgrC at a hydrophobic pocket formed within the transmembrane portion of α helices 4 and 8, areas that have been shown to shift during autophosphorylation of the AgrC protein[19]. While an earlier version of our study was publicly available as a preprint, a related study[42] showed the impact of testosterone on *S. aureus*. Our findings, using mice with epithelial-specific reductions of testosterone on the skin surface, bacterial transcriptomics and bioluminescent quorum-sensing models, add depth and context for all previous observations of sex-specific differences in *S. aureus* skin infection. These data provide definitive support for the direct sensing of testosterone by *S. aureus* and the function of this interaction in how *S. aureus* colonizes skin and causes skin damage. Although testosterone and DHT increase the virulence of *S. aureus*, other hormones such as progesterone, oestradiol and pregnenolone have no effect. Testosterone and DHT both have carbonyl and hydroxyl groups that extend beyond the steroid rings (Fig. 1d). The hormones that lack both moieties and have larger side chains are unable to stimulate quorum sensing, potentially explaining the differences in activity between hormone classes. These findings define testosterone and DHT as cues sensed by bacteria at the skin surface that regulate the expression of key virulence factors required for skin invasion and infection[12,13].

In contrast to progesterone and oestradiol that had a neutral effect on *S. aureus*, *ent*-T, a stereoisomer of testosterone, blocked the production of *psmα* and bacterially induced RBC and neutrophil killing. The

topical application of *ent*-T also inhibited *agr* quorum sensing in vivo. Therefore, *S. aureus* responds to testosterone in an enantioselective manner, with the natural testosterone generating activating signals and its chiral counterpart, *ent*-T, leading to inhibition of the same phenotypes. Notably, all sex steroids are found naturally in a single form and *ent*-steroids are chemically synthesized. The enantioselectivity of steroids has been reported for several other sex steroids in their interactions with G-protein-coupled receptors (GPCRs) and GABA (γ-aminobutyric acid) A receptors ($GABA_A$Rs) in the brain. At $GABA_A$Rs and GPCRs, natural sex steroids and their enantiomers bind to the same site of the protein, but demonstrate distinct effects on receptor signalling, which have been leveraged as therapeutics[39,40,43,44]. Our findings provide an example of this phenomenon in bacteria and the potential of *ent*-steroids for therapeutics.

The skin is known to generate antimicrobial proteins, antimicrobial lipids and nitric oxide that inhibit *S. aureus* pathogenesis[16,45,46]. Our work describes how the skin potentiates the infectious phenotypes of a pathogen at the skin surface through the secretion of androgens. Indeed, although the biosynthetic mutant had delayed kinetics in vitro (Fig. 3a), it retained the ability to sustain in vivo skin infections in mice with normal hormone production (Fig. 3g). Thus, the host-derived hormone signal is sufficient to activate *S. aureus* in vivo. In the in vivo biosynthetic mutant experiments, both exogenous testosterone and AIP-I only partially rescue luminescence (Fig. 3g). The rescue was probably not sustained due to the established instability of both AIP-I and testosterone in biological systems. AIPs contain a thiolactone ring and peptide backbone that are sensitive to oxidation and protease degradation, respectively[47,48]. Similarly, testosterone is actively metabolized in peripheral tissues such as the skin by enzymes including 17β-HSD and aromatase[49,50]. As a result, exogenous testosterone and AIP may not persist at biologically active levels in vivo. In contrast, endogenous production of AIP and testosterone, by *S. aureus* and the skin, respectively, allows continuous and localized accumulation of the signal, maintaining sustained *agr* activation over time (Figs. 1j and 3g). Taken together with our data showing that testosterone can directly stimulate *agr* (Fig. 2a) and augment AIP-I signalling (Fig. 3d and Extended Data Fig. 7d), the in vivo finding suggests that testosterone may be an initiating signal for *S. aureus* skin infection that is then sustained by AIPs generated by bacterial growth. These findings complement other examples of host hormones and cholesterol-derived molecules that supply activating interkingdom signals to microorganisms with which they have co-evolved, such as the ability of specific Gram-negative bacteria to respond to bile acids and adrenaline[51,52]. Our findings identify the ability of mammalian hormones to curate the virulence phenotypes of an opportunistic Gram-positive pathogen at the skin surface.

Given the capacity of skin androgens to cue the microbiota, our findings define the need for greater characterization of skin-secreted small molecules. These findings would also support the hypothesis that interventions that lower androgen amounts at the skin surface would improve the course of *S. aureus* infections, as we observed in the androgen-deficient mice (Fig. 1). We have previously quantified the secretion of skin sex steroids and illuminated topographic differences across the skin surface[5]. Previous work also shows that skin testosterone amounts shift during skin inflammation[53,54] and that IL-4 receptor signalling directly regulates androgen production through STAT6 binding to the HSD3B1 promoter[24]. Specific strains of *S. aureus* may also influence androgen amounts through sex steroid metabolism[55,56] and stimulation of IL-4 receptor signalling[30]. Therefore, therapeutic approaches that aim to regulate *S. aureus* virulence through inhibition of quorum sensing may need to take into account the concentration-dependent stimulation of quorum sensing by skin androgens[31,57]. Further, these findings suggest that the observed pathogenicity of *S. aureus* at the skin surface is an aggregate read-out of environmental signals generated from the host and signals generated by the microbiota[58].

Methods

Reagent and resource sharing

Reagents created for this study, including the *Hsd3b6*$^{\Delta skin}$ mice and bioluminescent strains of *S. aureus*, are available upon request from the corresponding author and may require a completed materials transfer agreement if there is potential for commercial application. Requests for resources should be directed to and will be fulfilled by the corresponding author.

Experimental model and participant details

Participant recruitment. This study was approved by the University of Texas (UT) Southwestern Institutional Review Board (STU 2019-0145), and written informed consent was obtained from study participants. Recruitment occurred from January 2024 to June 2024, and the human samples were collected between June 2024 and August 2024. Inclusion criteria included participants aged 18–40 years, a body mass index between 20 kg m^{-2} and 35 kg m^{-2}, and willingness and ability to comply with the requirements of the protocol. Exclusion criteria included participants outside the ages of 18–30 years, the use of antibiotics in the last 6 months, the use of topical medications, chronic skin disorders or other chronic medical conditions, the use of lipid or hormone-altering medications (except for oral contraceptives), the use of immunomodulator medications, women with irregular menstrual periods, or participants with a history of surgery to endocrine organs. Basic demographic and medical information was collected from each participant. Two healthy control participants, a 29-year-old male and a 26-year-old female, were selected and informed consent was obtained. Study participants were compensated in accordance with the approved study protocol.

Human skin sampling. Skin excretions were collected via Sebutape after completion of skin preparation to decrease external variables[5]. At the time of sampling, the forehead was cleaned with alcohol and four Sebutapes from Clinical and Derm LLC were applied for 15 minutes. Participants were sampled daily for 6 days between the hours of 12 PM and 3 PM. Following collection, tapes were stored in glass vials at −20 °C until processing. Hormones were extracted into 3 ml of LC–MS-grade methanol, and quantified via LC–MS/MS using a SCIEX QTRAP 6500+ (ref. 5). Outliers within the four biological replicate samples were identified using a dual-sided Grubbs' test, also called the extreme studentized deviate method, and were removed. The remaining biological replicate values for each day were averaged. These averaged values were translated from picogram per tape to nanomoles per litre (nM) using the total volume of the tape as provided in US patent US4532937A. Using GraphPad Prism v.10.4.1 (GraphPad Software), a linear regression model was created and plotted for each participant, along with the 95% confidence interval of each regression. An ordinary two-way analysis of variance (ANOVA) was performed to determine statistical significance of time and sex.

Human peripheral blood. Human peripheral blood samples were obtained from fully consented and institutional-review-board-approved donors through BioIVT, Innovative Research and IQ Biosciences.

Mice. Conventionally raised C57BL/6 male and female mice aged 6–9 weeks old were purchased from the Jackson Laboratory. C57BL/6 wild-type, *K14-Cre*$^{+/-}$ and *Hsd3b6*$^{fl/fl}$ (Extended Data Fig. 2a) mice were bred and maintained in the specific pathogen-free barrier facility at the UT Southwestern Medical Center at Dallas[59]. The generation of *Hsd3b6*$^{\Delta skin}$ (*K14-Cre*$^{+/-}$; *Hsd3b6*$^{fl/fl}$) is described below. Mice were co-housed with three to five mice per cage in all experiments. All mice were housed under a 12-hour light:12-hour dark cycle, at an ambient temperature of 22 ± 2 °C and relative humidity of 40–60%. Mice were fed ad libitum with free access to drinking water according to protocols approved by the Institutional Animal Care and Use Committees

of the UT Southwestern Medical Center. All experiments involving live animals were approved by the Institutional Animal Care and Use Committees of the UT Southwestern Medical Center (protocol number 2015-101064).

Hsd3b6$^{fl/fl}$ (C57BL/6), with *loxP* sites surrounding the first coding exon of *Hsd3b6*, were generated using CRISPR–Cas9 genome editing with guide RNAs targeting regions of the *Hsd3b6* locus (Extended Data Fig. 2a). Guide RNAs were injected into fertilized C57BL/6J embryos by the Children's Research Institute Mouse Genome Engineering facility at UT Southwestern. Healthy blastocytes were implanted in pseudo-pregnant mice. The resulting litter was screened by genomic sequencing to detect insertion of *loxP* sites and mice were bred to homozygosity and backcrossed with wild-type C57BL/6 mice. To generate *K14-Cre*$^{+/-}$; *Hsd3b6*$^{fl/fl}$ (*Hsd3b6*$^{\Delta skin}$) mice, *Hsd3b6*$^{fl/fl}$ mice were crossed with *K14-Cre*$^{+/-}$ mice to generate *K14-Cre*$^{+/-}$; *Hsd3b6*$^{fl/+}$ mice; *K14-Cre*; *Hsd3b6*$^{fl/+}$ mice were crossed to *Hsd3b6*$^{fl/fl}$ mice to obtain experimental mice *K14-Cre*$^{+/-}$; *Hsd3b6*$^{fl/fl}$ (*Hsd3b6*$^{\Delta skin}$) and corresponding controls, *Hsd3b6*$^{fl/fl}$. *Hsd3b6*$^{fl/fl}$ and *Hsd3b6*$^{\Delta skin}$ status was determined using PCR primers (Extended Data Table 2) and resolving on a 3% agarose gel.

Method details

Quantification of hormones in mouse samples. Age- (7–8 weeks) and sex-matched *Hsd3b6*$^{fl/fl}$ and *Hsd3b6*$^{\Delta skin}$ mice were analysed. Blood samples were obtained from the retro-orbital vein of anaesthetized mice followed by serum isolation with the micro sample tube Serum Gel (catalogue number 41.1378.005; Sarstedt). Skin hormones were quantified from skin secretions. After anaesthesia with isoflurane, hair was removed using depilatory cream and shaving. After 24 hours, Sebutape (Clinical and Derm LLC) was applied to the dorsal surface for 15 minutes (Extended Data Fig. 2e). Steroid extraction was performed as previously described[5]. Sebutape was removed and placed in 3 ml of chromatography–mass spectrometry grade methanol (catalogue number A456-500; Thermo Fisher Scientific) in an 8 ml polytetrafluorethylene/rubber-lined vial (catalogue number 03-343-3E; Thermo Fisher Scientific). The sample was then dried by vacuum centrifuge at 40 °C and stored at −20 °C until analysis. For analysis, samples were reconstituted with 100 µl of appropriate hormone kit assay buffer. Steroid hormone quantification of progesterone, testosterone and DHT was measured by mouse-specific immunoassay (catalogue numbers MBS7606191, MBS266250 and MBS760829; My BioSource) following the manufacturer's instructions.

Immunofluorescence microscopy. Mouse skin samples were fixed in formalin and embedded in paraffin by the UT Southwestern Histology Core. Samples were deparaffined with xylene followed by rehydration with decreasing concentrations of ethanol. Heat-induced antigen retrieval was attained in 10 mM sodium citrate buffer. Sections were washed briefly and blocked for an hour in blocking/permeabilization buffer (PBS, 5% goat serum and 0.5% Triton X-100). Sections were incubated in blocking/permeabilization buffer overnight with the following antibodies: anti-HSD3B6 (2.5 µg ml^{-1}; orb592071; Biorbyt), anti-cytokeratin-14 (1 µg ml^{-1}; sc-53253; Santa Cruz Biotechnology). After a brief wash in PBST (PBS + 0.2% Tween-20), sections were incubated with corresponding secondary antibodies: donkey anti-rabbit Alexa Fluor 647 (2 µg ml^{-1}; 711-605-152; Jackson Immunoresearch) and donkey anti-mouse Alexa Fluor 594 (2 µg ml^{-1}; A-21203; Thermo Fisher Scientific). The slides were then washed briefly in PBST and mounted with DAPI containing mounting medium (0100-20; SouthernBiotech). Images were processed using a Zeiss 780 confocal microscope.

Bacterial strains and plasmids. *S. aureus* strains (Extended Data Table 1) were streaked on tryptic soy agar plates and grown overnight at 37 °C. Single colonies were selected and cultured in tryptic soy broth (TSB) at 150 rpm at 37 °C in a shaking incubator overnight, followed by a 1:100 subculture at 37 °C in a shaking incubator to obtain bacteria from the mid-log phase (optical density at 600 nm ($OD_{600\,nm}$) = 0.6). For reporter strains, all in vitro cultures were performed using TSB in the presence of 10 µg ml^{-1} of chloramphenicol. Bacteria were pelleted, washed with PBS and resuspended in either TSB for in vitro experiments or PBS for in vivo experiments. HG003, Δ*agrC*, Δ*agrBD* and Δ*agrA* mutant strains were obtained from Dr Ferric Fang, University of Washington School of Medicine[16]. *S. aureus* strains from AD skin were obtained from Dr Julie Segre and Dr Heidi Kong[30]. All other strains from the collections of the laboratories of A.R.H. and T.A.H.-T.

Construction of *lux*-expressing strains. The integrated *luxCDABEG* cassette was transduced into *S. aureus* strains HG003, Δ*agrBD* and Δ*agrC* obtained from the laboratory of Dr. Ferric Fang, University of Washington School of Medicine[16,40] using phage 11 generating strains AH6222 (*lux*+), AH6224 (*lux*+) and AH6223 (*lux*+), respectively.

Construction of complemented Δ*agrC* strain. The HG003 Δ*agrC* strain was complemented by introducing the pAgrC1AgrA plasmid[60] by phage transduction[61] using phage 11.

In vitro luminescence assays. *S. aureus* strains, HG003, Δ*agrBD* and Δ*agrC* with constitutive Lux (φ11::LL29*luxCDABEG*) and quorum-sensing-dependent lux (pAmiAgrP3lux) plasmids (HG003 (AH6225) *agr* type I, USA100 (AH430) MRSA type II and MW2 (AH1747) MRSA type III)[14,18] were grown in TSB supplemented with antibiotic selection and subcultured 1:200 into fresh TSB containing steroid hormone. The assay was completed in opaque-sided, 96-well, clear-bottom, tissue-culture-treated plates with a final well volume of 200 µl. Bioluminescent signals (photons per 0.1 second acquisition time) were measured using a BioTek H1 Synergy plate reader. Experiments were completed in triplicate, with the *agr*-type-specific AIPs AIP-I (catalogue number 4515-v; Peptide Institute), AIP-II (catalogue number 4516-v; Peptide Institute) and AIP-III (catalogue number 4517-v; Peptide Institute) as positive control.

In vitro growth assay. *S. aureus* strains HG003 (*agr* type I), Δ*agrBD*, Δ*agrC*, USA100 (AH430; MRSA type II) and MW2 (AH1747; MRSA type III) were cultured overnight in TSB at 37 °C with shaking. Overnight cultures were diluted 1:100 in fresh TSB and grown to mid-log phase. Bacterial suspensions were inoculated into 96-well clear-bottom plates containing 10 nM testosterone, 10 nM DHT or vehicle control. OD_{600} was measured over a 24-hour incubation period to assess bacterial growth using a BioTek H1 Synergy plate reader.

Haemolysis assay. Overnight cultures of HG003, Δ*agrBD* and Δ*agrC* strains were inoculated 1:200 into 10 ml of TSB containing testosterone, AIP-I or vehicle alone at concentrations of 10 nM. Cells were grown to mid-log phase. The supernatant of 1 ml of culture was filter sterilized using Millex sterile syringe filters with a pore size of 0.22 µm (catalogue number SLGV033RS). Filtered supernatant diluted 1:1 with PBS was added to 25 µl of human blood (catalogue numbers HUMANWBK2-0110649 and HUMANWBK2-0110717; BioIVT; catalogue number IWB1K2E-10ML; Innovative Research) to a 96-well V-bottom plate and incubated with agitation at 37 °C for 1 hour. After spinning at 1,000 rpm for 10 minutes, the supernatant was transferred to a flat-bottom 96-well plate. Absorbance was read at 541 nm (A_{541}) for haemoglobin using a BioTek H1 Synergy plate reader. The percentage of haemolysis was calculated using the following formula: (A_{541} of RBC-treated sample − A_{541} of buffer)/(A_{541} of H_2O − A_{541} of buffer); where buffer (PBS) = baseline, H_2O = 100% haemolysis[70].

Skin cell cytotoxicity assay. Cultures of HG003, Δ*agrBD* and Δ*agrC* strains were grown overnight with TSB containing testosterone, AIP-I or vehicle alone at concentrations of 10 nM. Bacteria were pelleted, followed by filter sterilization of the supernatant using Millex

sterile syringe filters with a pore size of 0.22 µm (catalogue number SLGV033RS). Human keratinocytes (HaCaT cells; catalogue number T0020001; AddexBio) were used for cytotoxicity assays. These cells are spontaneously transformed keratinocytes derived from histologically normal skin of a male donor (62 years old). Cells were cultured in AddexBio-optimized DMEM supplemented with 10% FBS under standard conditions. HaCaT cells were treated with sterile-filtered bacterial supernatants at 5% by volume for 24 hours. After PBS washing, the resulting supernatants were used to measure lactate dehydrogenase (LDH) release from damaged cells using the LDH Cytotoxicity Detection Kit (catalogue number 2570393; Invitrogen).

Neutrophil killing assay. HG003, Δ*agrBD* and Δ*agrC* strains of bacteria were treated with testosterone, AIP-I or vehicle at concentrations of 10 nM and allowed to grow to mid-log phase (OD_{600} = 0.6). Purified human neutrophils (catalogue number IQB-Hu1-Nu10; IQ Biosciences; catalogue numbers HUMANNEUT-0127862 and HUMANNEUT-0127879; BioIVT) were seeded at 1×10^5 cells per well into a 96-well plate in 90 µl of RPMI. Bacterial supernatants (10 µl) were added (final concentration of 10%). After 3 hours incubation at 37 °C, 5% CO_2, the plates were centrifuged at 250*g* for 10 minutes, and the resulting supernatants were used to measure LDH leakage from damaged cells as the marker of neutrophil lysis with an LDH Cytotoxicity Detection Kit (catalogue number 2570393; Invitrogen). The percentage of neutrophil lysis was calculated using neutrophils incubated with 10% RPMI as 0% lysis control, and neutrophils incubated with 0.2% Triton X-100 were defined as 100% lysis[71].

Quantitative real-time PCR. HG003, USA100 (AH3684), MW2 (AH843), Δ*agrBD,* Δ*agrA*, Δ*agrC* and AD strains were treated with testosterone and/or the respective AIPs at concentrations of 10 nM and allowed to grow to mid-log phase. Cells were pelleted and lysed using lysis matrix B tubes containing 0.1 mm silica spheres (catalogue number 174701; MP Lysing Matrix Tubes) and lysostaphin (catalogue number L7386; Sigma) at room temperature, and RNA was purified using the RNeasy Mini Kit (catalogue number 74104; Qiagen). RNA was quantified by absorbance at 260 nm, and its purity was evaluated by the ratios of absorbance at 260 nm:280 nm. RNA was used as a template to generate cDNA using the High-Capacity Reverse Transcription Kit (catalogue number 01071619; Applied Biosystems). Quantitative real-time PCR was performed by amplifying cDNA using Power SYBR Green Master Mix (catalogue 2749999; Applied Biosystems) and QuantStudio 7 Flex Real-Time PCR System (Applied Biosystems). Relative expression values were calculated using the comparative Ct (ΔΔCt) method, and transcript abundances were normalized to *gyrA* transcript abundance for *S. aureus* and *Rplp0* for mouse tissue samples. Primer sequences are shown in Extended Data Table 2.

RNA sequencing. Briefly, cultures of HG003 were grown in TSB with 10 nM or 100 nM of testosterone, 10 nM pregnenolone or DMSO alone in triplicate to an optical density of 0.4 at OD_{600}. Cells were collected and treated with RNA Protect Bacteria Reagent (catalogue number 76526; Qiagen). Cells were lysed using lysostaphin (catalogue number L7386; Sigma) and RNA purified using the RNeasy Mini Kit (catalogue number 74104; Qiagen). Sample quality was affirmed via Bioanalyzer (Agilent). Ribosomal RNA was depleted using RiboCop from the Bacterial META Removal Kit (Lexogen). cDNA libraries were generated at the University of Michigan Microbiome core using the CORALL RNA-seq Library Prep Kit (Lexogen). Samples were barcoded, pooled and sequenced in 125 × 125 paired-end reads on an Illumina HiSeq 2000 sequencer. Raw sequencing reads in FASTQ format were aligned and annotated to the *S. aureus* NCTC8325 reference genome with annotated small RNA[62] using QiagenCLC Genomics Workbench default settings (v.21.0.5): mismatch cost, 2; insertion and deletion cost, 3; length and similarity fraction, 0.8. Normalization and differential expression calculations of uniquely mapped bacterial transcripts were performed using CLC. All transcripts with a false-discovery-rate-adjusted $P < 0.05$ were considered significant.

***S. aureus* epicutaneous skin infections.** Before infection studies, mice were acclimatized to the animal biosafety level 2 animal housing facility. Age- (7–8 weeks), strain- and sex-matched C57BL/6 male and female mice, *Hsd3b6*$^{fl/fl}$ and *Hsd3b6*$^{\Delta skin}$ were used in the study. A previously described mouse model of epicutaneous *S. aureus* exposure was followed[21,46]. Briefly, the dorsal skin of anaesthetized mice (2% isoflurane) was shaved and depilated (Nair cream). After 24 hours, bioluminescent *S. aureus* strains were grown to mid-log phase, pelleted and resuspended in PBS to achieve inoculum containing 1×10^6 CFU. A 100 µl volume of PBS containing 1×10^6 CFU with or without 10 nmoles of testosterone, AIP-I or the same volume of vehicle was placed on a sterile gauze pad and attached to the shaved skin with transparent bio-occlusive dressing (catalogue number 1622W; Tegaderm 3M; Henry Schein Medicals), and secured with adhesive bandages (catalogue number 1275033; Band-Aid; Johnson & Johnson, American White Cross) for 4 days. Photons emitted from luminescent bacteria were collected during an auto-exposure using the IVIS Lumina 3 imager machine and living image software (Xenogen) over the course of 1 minute. Bioluminescent image data are presented on a pseudo-colour scale (blue representing least intense and red representing the most intense signal) overlaid onto a greyscale photographic image. Using the image analysis tools in living image software, circular analysis windows (of uniform area) were overlaid onto dorsal regions of the infection area, and the corresponding bioluminescence values (total flux) were measured and plotted versus time after infection. Mice were randomly assigned to treatment groups, and at experimental endpoints, mice were euthanized using carbon dioxide inhalation.

Disease scoring. The severity of skin inflammation was assessed by a blinded observer from digital photographs and the total disease score was quantified[21]. The sum of the individual grades for erythema, oedema, erosion and scaling were each graded as 0 (none), 1 (mild), 2 (moderate) or 3 (severe).

Transepidermal water loss measurement. Transepidermal water loss, a measure of barrier function and integrity, of mice dorsal skin was measured using Vapometer (Delfin Technologies) according to manufacturer instructions[63].

Histology. Skin biopsy specimens were collected, fixed in 10% formalin and paraffin embedded. Skin cross-sections of 4 µm were mounted onto glass slides and stained with haematoxylin and eosin by the UT Southwestern Histology Core, according to guidelines for clinical samples. Epidermal thickness was measured by taking ten epidermal thickness measurements per mouse, averaged from images (Echo Revolve Microscopy) using ImageJ software.

Measurement of quorum sensing in vivo. *S. aureus* strains expressing quorum-sensing lux (pAmiAgrP3lux) plasmids were grown in TSB medium containing chloramphenicol overnight at 37 °C in a shaking incubator set to 150 rpm. Overnight cultures were diluted 1:100 TSB with chloramphenicol to mid-log phase and then pelleted and washed 2× in PBS and resuspended in sterile saline. PBS inoculum suspensions (100 µl) containing 1×10^6 CFU were placed on a sterile gauze pad (1 cm × 1 cm) and attached to the shaved skin with transparent bio-occlusive dressing, with or without testosterone, *ent*-T, AIP-I or vehicle (3M; Tegaderm) and secured with 2 layers of adhesive bandages (Band-Aid; Johnson & Johnson). Beginning immediately after infection, mice were imaged hourly under isoflurane inhalation anaesthesia (2%). Photons emitted from luminescent bacteria were collected during auto-exposure using the IVIS Lumina 3 imager machine and living

image software (Xenogen). Corresponding bioluminescence values (total flux) were measured and plotted versus time after infection[40].

In silico docking of testosterone to the AgrC receptor. The dimeric structure of AgrC was predicted using AlphaFold 2 (refs. 33,34) as implemented in Google Colab. The sensory domain of a single subunit (residues 1–207) was selected for ligand docking. AIP-I was docked in silico using SwissDock[35,37] with nuclear-magnetic-resonance-derived coordinates for AIP-I. The docking pose for AIP-I that best aligned with reported structure–activity relationships[11,41] was selected as the AgrC–AIP-I complex for subsequent steroid docking. Stereospecific compound templates were retrieved from PubChem (testosterone; compound identifier 6013). Initial docking produced an AgrC model featuring a depression on the sensory domain surface, consistent with a putative membrane-exposed ligand-binding pocket. To refine the complex, co-folding of AgrC in the presence of both AIP-I and testosterone was performed using AF3[64], implemented in PXDesign[65,66] on the Protenix Server (https://protenix-server.com). AF3 successfully docked both ligands but introduced stereochemical distortions consistent with known AF3 limitations[64]. These effects were also reproduced using Boltz-2 (ref. 67). To correct for these artefacts, the co-folded AgrC–AIP-I complex was used as the target for in silico docking of testosterone with an updated version of AutoDock Vina[68,69]. All structures were visualized and analysed using PyMOL v.2.5.2 (Schrödinger).

Quantification and statistical analysis

Statistical details of experiments can be found in the figure legends, including how significance was defined and the statistical methods used. Data represent mean ± s.e.m. Formal randomization techniques were not used; however, mice were allocated to experiments randomly. Mice that were determined to be in the anagen hair cycle at the initiation of the experiment were excluded. All statistical analyses were performed with GraphPad Prism software (v.10.0.1), except the bioluminescent imaging data that was analysed as described above. To assess the statistical significance of the difference between two treatments for in vitro models, we used unpaired two-tailed Student's *t*-tests. To assess the statistical significance of the difference between two treatments for mouse models, we used the Mann–Whitney *U*-test and Kolmogorov–Smirnov test. To assess the statistical significance of differences between more than two treatments in vitro, we used one-way ANOVA with post-test corrections. To assess the statistical significance of differences between more than two treatment groups in mouse models, we used the Kruskal–Wallis test with post-test corrections. For experiments in vitro and in vivo where metrics were calculated over time, we used two-way ANOVA with post-test corrections. For the RNA-sequencing experiments, expression data were analysed with CLC. All transcripts with a false-discovery-rate-adjusted $P < 0.05$ were considered significant.

Reporting summary. Further information on research design is available in the Nature Portfolio Reporting Summary linked to this article.

Data availability

Sequencing data have been submitted to the National Center for Biotechnology Information Sequence Read Archive under BioProject accession number PRJNA1071176. Source data are provided with this paper.

Code availability

No unique code was generated for this study.

References

1. Stensen, D. B. et al. Circulating sex-steroids and *Staphylococcus aureus* nasal carriage in a general female population. *Eur. J. Endocrinol.* **184**, 337–346 (2021).
2. Ricardo Vázquez-Martínez, E., García-Gómez, E., Camacho-Arroyo, I. & González-Pedrajo, B. Sexual dimorphism in bacterial infections. *Biol. Sex Differ.* https://doi.org/10.1186/s13293-018-0187-5 (2018).
3. Castleman, M. J. et al. Innate sex bias of *Staphylococcus aureus* skin infection is driven by α-hemolysin. *J. Immunol.* **200**, 657–668 (2018).
4. Hammes, S. R. & Levin, E. R. Impact of estrogens in males and androgens in females. *J. Clin. Invest.* **129**, 1818–1826 (2019).
5. Pineider, J., Eckert, K. M., McDonald, J. G. & Harris-Tryon, T. Cutaneous hormone production is distinct between anatomical sites and between males and females. *J. Invest. Dermatol.* **143**, 596–601 (2023).
6. Sturges, C. I. et al. Cutaneous hormone sampling and analysis for dermatologic research. *J. Invest. Dermatol.* **145**, 1850–1857 (2025).
7. Miller, L. G. et al. Incidence of skin and soft tissue infections in ambulatory and inpatient settings, 2005–2010. *BMC Infect. Dis.* **15**, 362 (2015).
8. Severn, M. M. et al. The ubiquitous human skin commensal *Staphylococcus hominis* protects against opportunistic pathogens. *mBio* **13**, e0093022 (2022).
9. Chen, Y. E., Fischbach, M. A. & Belkaid, Y. Skin microbiota–host interactions. *Nature* https://doi.org/10.1038/nature25177 (2018).
10. Byrd, A. L., Belkaid, Y. & Segre, J. A. The human skin microbiome. *Nat. Rev. Microbiol.* **16**, 143–155 (2018).
11. Jenul, C. & Horswill, A. R. Regulation of *Staphylococcus aureus* virulence. *Microbiol. Spectr.* https://doi.org/10.1128/microbiolspec.gpp3-0031-2018 (2019).
12. Nakagawa, S. et al. *Staphylococcus aureus* virulent PSMα peptides induce keratinocyte alarmin release to orchestrate IL-17-dependent skin inflammation. *Cell Host Microbe* **22**, 667–677 (2017).
13. Nakamura, Y. et al. *Staphylococcus* Agr virulence is critical for epidermal colonization and associates with atopic dermatitis development. *Sci. Transl. Med.* **12**, eaay4068 (2020).
14. Hall, P. R. et al. Nox2 modification of LDL is essential for optimal apolipoprotein B-mediated control of agr type III *Staphylococcus aureus* quorum-sensing. *PLoS Pathog.* **9**, e1003166 (2013).
15. Rothfork, J. M. et al. Inactivation of a bacterial virulence pheromone by phagocyte-derived oxidants: new role for the NADPH oxidase in host defense. *Proc. Natl Acad. Sci. USA* **101**, 13867–13872 (2004).
16. Urbano, R. et al. Host nitric oxide disrupts microbial cell-to-cell communication to inhibit staphylococcal virulence. *Cell Host Microbe* **23**, 594–606.e7 (2018).
17. Baba, T. et al. Genome and virulence determinants of high virulence community-acquired MRSA. *Lancet* **359**, 1819–1827 (2002).
18. Grundstad, M. L. et al. Quorum sensing, virulence, and antibiotic resistance of USA100 methicillin-resistant *Staphylococcus aureus* isolates. *mSphere* **4**, e00553-19 (2019).
19. Wang, B., Zhao, A., Novick, R. P. & Muir, T. W. Activation and inhibition of the receptor histidine kinase AgrC occurs through opposite helical transduction motions. *Mol. Cell* **53**, 929–940 (2014).
20. Stensen, D. B. et al. Circulating sex-steroids and *Staphylococcus aureus* nasal carriage in a general male population. *Epidemiol. Infect.* **150**, e93 (2022).
21. Liu, H. et al. *Staphylococcus aureus* epicutaneous exposure drives skin inflammation via IL-36-mediated T cell responses. *Cell Host Microbe* **22**, 653–666.e5 (2017).
22. Wu, G. et al. Variant allele of HSD3B1 increases progression to castration-resistant prostate cancer. *Prostate* https://doi.org/10.1002/pros.22967 (2015).

23. Simard, J. et al. Molecular biology of the 3β-hydroxysteroid dehydrogenase/ Δ^5-Δ^4 isomerase gene family. *Endocr. Rev.* **26**, 525–582 (2005).
24. Zhang, C. et al. Interleukins 4 and 13 drive lipid abnormalities in skin cells through regulation of sex steroid hormone synthesis. *Proc. Natl Acad. Sci. USA* **118**, e2100749118 (2021).
25. Marroquin, S. et al. MroQ is a novel Abi-domain protein that influences virulence gene expression in *Staphylococcus aureus* via modulation of agr activity. *Infect. Immun.* **87**, e00002-19 (2019).
26. Parlet, C. P. et al. Apicidin attenuates MRSA virulence through quorum-sensing inhibition and enhanced host defense. *Cell Rep.* **27**, 187–198.e6 (2019).
27. Abbasian, S. et al. Genotypic characterization of *Staphylococcus aureus* isolated from a burn centre by using *agr*, *spa* and SCC mec typing methods. *New Microbes New Infect.* **26**, 15–19 (2018).
28. Kong, H. H. et al. Temporal shifts in the skin microbiome associated with disease flares and treatment in children with atopic dermatitis. *Genome Res.* **22**, 850–859 (2012).
29. Paller, A. S. et al. The microbiome in patients with atopic dermatitis. *J. Allergy Clin. Immunol.* **143**, 26–35 (2019).
30. Byrd, A. L. et al. *Staphylococcus aureus* and *S. epidermidis* strain diversity underlying human atopic dermatitis. *Sci. Transl. Med.* **9**, eaal4651 (2017).
31. Nakatsuji, T. et al. Development of a human skin commensal microbe for bacteriotherapy of atopic dermatitis and use in a phase 1 randomized clinical trial. *Nat. Med.* **27**, 700–709 (2021).
32. Rutherford, S. T. & Bassler, B. L. Bacterial quorum sensing: its role in virulence and possibilities for its control. *Cold Spring Harb. Perspect. Med.* **2**, a012427 (2012).
33. Jumper, J. et al. Highly accurate protein structure prediction with AlphaFold. *Nature* **596**, 583–589 (2021).
34. Mirdita, M. et al. ColabFold: making protein folding accessible to all. *Nat. Methods* **19**, 679–682 (2022).
35. Grosdidier, A., Zoete, V. & Michielin, O. Fast docking using the CHARMM force field with EADock DSS. *J. Comput. Chem.* **32**, 2149–2159 (2011).
36. Tal-Gan, Y., Ivancic, M., Cornilescu, G., Cornilescu, C. C. & Blackwell, H. E. Structural characterization of native autoinducing peptides and abiotic analogues reveals key features essential for activation and inhibition of an AgrC quorum sensing receptor in *Staphylococcus aureus*. *J. Am. Chem. Soc.* **135**, 18436–18444 (2013).
37. Sterling, T. & Irwin, J. J. ZINC 15—ligand discovery for everyone. *J. Chem. Inf. Model.* **55**, 2324–2337 (2015).
38. Crowley, J., Withana, M. & Deplazes, E. The interaction of steroids with phospholipid bilayers and membranes. *Biophys. Rev.* **14**, 163–179 (2022).
39. Covey, D. F. ent-Steroids: novel tools for studies of signaling pathways. *Steroids* **74**, 577–585 (2009).
40. Covey, D. F. et al. Neurosteroid enantiomers as potentially novel neurotherapeutics. *Neurosci. Biobehav. Rev.* **149**, 105191 (2023).
41. Thoendel, M., Kavanaugh, J. S., Flack, C. E. & Horswill, A. R. Peptide signaling. in the staphylococci. *Chem. Rev.* **111**, 117–151 (2011).
42. Luo, Z. et al. The role of male hormones in bacterial infections: enhancing *Staphylococcus aureus* virulence through testosterone-induced Agr activation. *Arch. Microbiol.* **206**, 401 (2024).
43. Biellmann, J. F. Enantiomeric steroids: synthesis, physical, and biological properties. *Chem. Rev.* **103**, 2019–2033 (2003).
44. Katona, B. W. et al. Neurosteroid analogues. 12. Potent enhancement of GABA-mediated chloride currents at GABAA receptors by ent-androgens. *Eur. J. Med. Chem.* **43**, 107–113 (2008).
45. Harris-Tryon, T. A. & Grice, E. A. Microbiota and maintenance of skin barrier function. *Science* **376**, 940–945 (2022).
46. Zhang, C. et al. Small proline-rich proteins (SPRRs) are epidermally produced antimicrobial proteins that defend the cutaneous barrier by direct bacterial membrane disruption. *eLife* **11**, e76729 (2022).
47. Montagut, E. J. et al. Direct quantitative immunochemical analysis of autoinducer peptide IV for diagnosing and stratifying *Staphylococcus aureus* infections. *ACS Infect. Dis.* **8**, 645 (2022).
48. Verbeke, F. et al. Peptides as quorum sensing molecules: measurement techniques and obtained levels in vitro and in vivo. *Front. Neurosci.* **11**, 183 (2017).
49. Thiboutot, D. et al. Human skin is a steroidogenic tissue: steroidogenic enzymes and cofactors are expressed in epidermis, normal sebocytes, and an immortalized sebocyte cell line (SEB-1). *J. Invest. Dermatol.* **120**, 905–914 (2003).
50. Chen, W., Zouhoulis, C. C. & Orfanos, C. E. The 5 alpha-reductase system and its inhibitors. Recent development and its perspective in treating androgen-dependent skin disorders. *Dermatology* **193**, 177–184 (1996).
51. Pacheco, A. R. & Sperandio, V. Inter-kingdom signaling: chemical language between bacteria and host. *Curr. Opin. Microbiol.* **12**, 192–198 (2009).
52. Zou, A. J. et al. Molecular determinants for differential activation of the bile acid receptor from the pathogen *Vibrio parahaemolyticus*. *J. Biol. Chem.* **299**, 104591 (2023).
53. Pyle, H. J. et al. Assessment of the cutaneous hormone landscapes and microbiomes in vulvar lichen sclerosus. *J. Invest. Dermatol.* https://doi.org/10.1016/J.JID.2024.01.027 (2024).
54. Haag, M. et al. Age and skin site related differences in steroid metabolism in male skin point to a key role of sebocytes in cutaneous hormone metabolism. *Dermato-endocrinology* **4**, 58–64 (2012).
55. Zhou, X. et al. High abundance of testosterone and salivary androgen-binding protein in the lateral nasal gland of male mice. *J. Steroid Biochem. Mol. Biol.* **117**, 81–86 (2009).
56. Xiang, G. et al. Nasal *Staphylococcus aureus* carriage promotes depressive behaviour in mice via sex hormone degradation. *Nat. Microbiol.* **10**, 2425–2440 (2025).
57. Nakatsuji, T. et al. Antimicrobials from human skin commensal bacteria protect against *Staphylococcus aureus* and are deficient in atopic dermatitis. *Sci. Transl. Med.* **9**, eaah4680 (2017).
58. Williams, M. R. et al. Quorum sensing between bacterial species on the skin protects against epidermal injury in atopic dermatitis. *Sci. Transl. Med.* **11**, eaat8329 (2019).
59. Sampath, H. et al. Skin-specific deletion of stearoyl-CoA desaturase-1 alters skin lipid composition and protects mice from high fat diet-induced obesity. *J. Biol. Chem.* **284**, 19961–19973 (2009).
60. Jensen, R. O., Winzer, K., Clarke, S. R., Chan, W. C. & Williams, P. Differential recognition of *Staphylococcus aureus* quorum-sensing signals depends on both extracellular loops 1 and 2 of the transmembrane sensor AgrC. *J. Mol. Biol.* **381**, 300–309 (2008).
61. Novick, R. P. Genetic systems in Staphylococci. *Methods Enzymol.* **204**, 587–636 (1991).
62. Carroll, R. K. et al. Genome-wide annotation, identification, and global transcriptomic analysis of regulatory or small RNA gene expression in *Staphylococcus aureus*. *mBio* **7**, e01990-15 (2016).
63. Amano, T., Takeda, T., Yano, H. & Tamura, T. Olopatadine hydrochloride accelerates the recovery of skin barrier function in mice. *Br. J. Dermatol.* **156**, 906–912 (2007).
64. Abramson, J. et al. Accurate structure prediction of biomolecular interactions with AlphaFold 3. *Nature* **630**, 493–500 (2024).

65. Protenix Team et al. PXDesign: fast, modular, and accurate de novo design of protein binders. Preprint at *bioRxiv* https://doi.org/10.1101/2025.08.15.670450 (2025).
66. ByteDance AML AI4Science Team et al. Protenix—advancing structure prediction through a comprehensive AlphaFold3 reproduction. Preprint at *bioRxiv* https://doi.org/10.1101/2025.01.08.631967 (2025).
67. Passaro, S. et al. Boltz-2: towards accurate and efficient binding affinity prediction. Preprint at *bioRxiv* https://doi.org/10.1101/2025.06.14.659707 (2025).
68. Eberhardt, J., Santos-Martins, D., Tillack, A. F. & Forli, S. AutoDock Vina 1.2.0: new docking methods, expanded force field, and python bindings. *J. Chem. Inf. Model.* **61**, 3891–3898 (2021).
69. Bugnon, M. et al. SwissDock 2024: major enhancements for small-molecule docking with Attracting Cavities and AutoDock Vina. *Nucleic Acids Res.* **52**, W324–W332 (2024).
70. Rowe, G. E. & Welch, R. A. Assays of hemolytic toxins. *Methods Enzymol.* **235**, 657–667 (1994).
71. Kwiecinski, J. M. et al. *Staphylococcus aureus* uses the ArlRS and MgrA cascade to regulate immune evasion during skin infection. *Cell Rep.* **36**, 109462 (2021).

Acknowledgements

We thank A. Croft for discussions and aid in experimental design. This work was supported by National Institutes of Health grant NIAMS-K08AR076459 (T.A.H.-T.), NIAID-AI162964 (A.R.H.), NIAID-AI153185 (A.R.H.), VA Merit Award BX002711 (A.R.H.), Burroughs Wellcome Fund 1022777 (T.A.H.-T.) and NIAID-AI187273 (A.R.H. and T.A.H.-T.).

Author contributions

Conceptualization: T.A.H.-T., M.S.J., J.S.K., A.R.H. and J.G.M. Methodology: T.A.H.-T., M.S.J., M.B., J.S.K., T.S. and J.G.M. Investigation: M.S.J., M.C., T.S., M.A., C.I.S., M.B., R.A.K., J.S.K., M.V., H.G., J.K., S.J. and T.A.H.-T. Visualization: M.S.J., T.A.H.-T., C.I.S., T.S., R.A.K. and J.S.K. Funding acquisition: T.A.H.-T. and A.R.H. Project administration: T.A.H.-T. Supervision: T.A.H.-T., A.R.H. and J.G.M. Writing—original draft: T.A.H.-T. and M.S.J. Writing—review and editing: T.A.H.-T., M.S.J., M.C., C.I.S., M.B., T.S., J.S.K. and A.R.H.

Competing interests

T.A.H.-T., M.S.J., A.R.H. and J.K. have filed a patent (US patent application number 63/580,813). Mirofend L.L.C. (founder, T.A.H.-T.). The other authors declare no competing interests.

Additional information

Extended data is available for this paper at https://doi.org/10.1038/s41564-026-02261-2.

Supplementary information The online version contains supplementary material available at https://doi.org/10.1038/s41564-026-02261-2.

Correspondence and requests for materials should be addressed to Tamia A. Harris-Tryon.

Peer review information *Nature Microbiology* thanks Andreas Peschel and the other, anonymous, reviewer(s) for their contribution to the peer review of this work. Peer reviewer reports are available.

https://doi.org/10.1038/s41564-026-02261-2

Extended Data Table 1 | *Staphylococcus aureus* strains used in this work

S. aureus strains	Reference	Identifier
HG003	PMID: 29706505	RU083
USA100	PMID: 30943400	AH3684
MW2	PMID: 30943400	AH843
HG003-Δ*agrA*	PMID: 29706505	RU111
HG003-Δ*agrC*	PMID: 29706505	RU141
HG003-Δ*agrBD*	PMID: 29706505	RU299
MRSA SAP430::luxABCDE	PMID: 29120743	*Staphylococcus aureus* USA300 LAC::lux
HG003, φ11::LL29luxCDABEG	This work	AH6222
HG003-Δ*agrBD*, φ11::LL29luxCDABEG	This work	AH6224
HG003-Δ*agrC*, φ11::LL29luxCDABEG	This work	AH6223
USA300 LAC + pAmiAgrP3lux (camR)	PMID: 30943400	AH2759
HG003+ pAmiAgrP3lux (camR)	This work	AH6225
USA100 IA116 + pAmiAgrP3lux (camR)	PMID: 30943400	AH4390
MW2+ pAmiAgrP3lux (camR)	PMID: 31413175	AH3185
HG003-Δ*agrBD* + pAmiAgrP3lux (camR)	This work	AH6227
HG003-Δ*agrC*+ pAmiAgrP3lux (camR)	This work	AH6226
HG003-Δ*agrC*+ pAgrC1AgrA plasmid (camR)	This work	AH6504

https://doi.org/10.1038/s41564-026-02261-2

Extended Data Table 2 | Primers for Quantitative RT-PCR and Gene Sequencing

Gene	Species	Sequence, 5'→3'	Ref.
gyrA	*Staphylococcus aureus*	Forward: AAGGTGTTCGCTTAATTCGCReverse: ATTGCATTTCCTGGTGTTTC	PMID: 21926198
psma	*Staphylococcus aureus*	Forward: TATCAAAAGCTTAATCGAACAATTCReverse: CCCCTTCAAATAAGATGTTCATATC	PMID: 21926198
hla	*Staphylococcus aureus*	Forward : GGGGACCATATGATAGAGATTReverse: TGTAGCGAAGTCTGGTGAAA	PMID: 21926198
lukS-PV	*Staphylococcus aureus*	Forward: ATGAGGTGGCCTTTCCAATACReverse: CCTGTTGATGGACCACTATTA	PMID: 21926198
RNAIII	*Staphylococcus aureus*	Forward: CGATGTTGTTTACGATAGCTTReverse: CCATCCCAACTTAATAACCA	PMID: 21926198
hld	*Staphylococcus aureus*	Forward: GAGTTGTTTAATTTTAAGReverse: TTTTAGTGAATTTGT	PMID: 27917374
agrA	*Staphylococcus aureus*	Forward: GAAGACGATCCAAAACAAAGAGReverse: GTCATTCATATTTTTAGCTTGCTC	PMID: 29706505
Hsd3b6-Full	*Mus musculus*	Forward: CCCAGAGACCATCCTTTATGTCReverse: CTCTCCCTGTCTCCTTACATTTC	
Hsd3b6-Left	*Mus musculus*	Forward: CCCAGAGACCATCCTTTATGTCReverse: CAAACCTCCCATAGCACAGAT	This work
Hsd3b6-Right	*Mus musculus*	Forward: GGGATCCTCCCTTGTCTAGTAReverse: CTCTCCCTGTCTCCTTACATTTC	This work
Cre- MUC	*Mus musculus*	Forward: CTTCTATATCTTCAGGCGCGCGGTCTGGCAReverse: TTTTCTGACCCGGCAAAACAGGTAGTTATTCGG	
*Hsd3b6*_Exon1	*Mus musculus*	Forward: ATGCCTGGGTGGAGCTGReverse: CCCTGATCTCCTCCAGATCTTTC	This work
Rplp0	*Mus musculus*	Forward: AGATTCGGGATATGCTGTTGGCReverse: TCGGGTCCTAGACCAGTGTTC	

https://doi.org/10.1038/s41564-026-02261-2

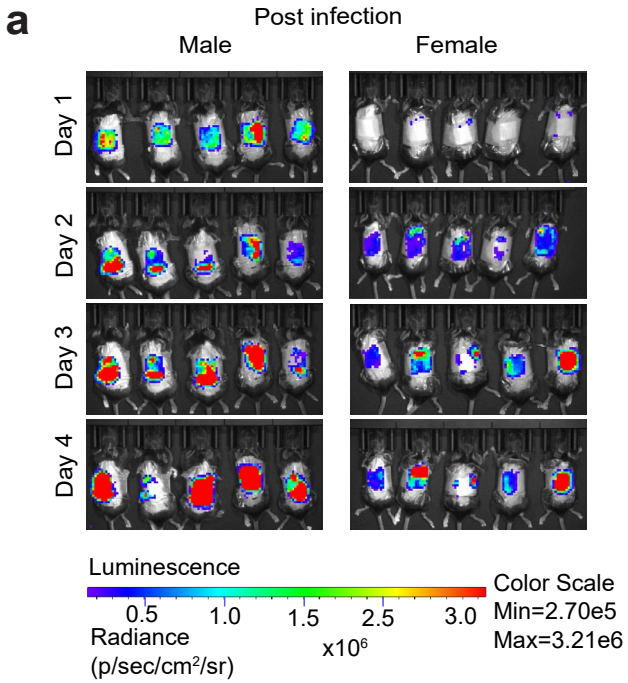

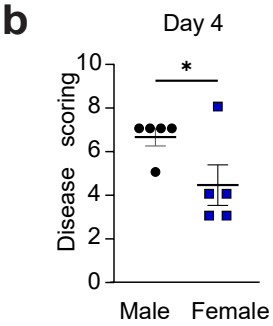

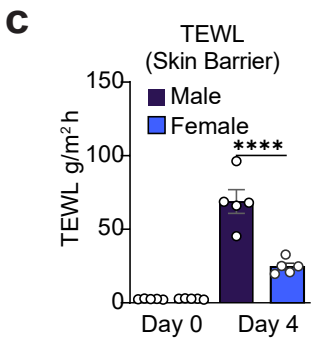

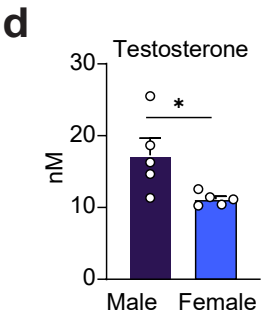

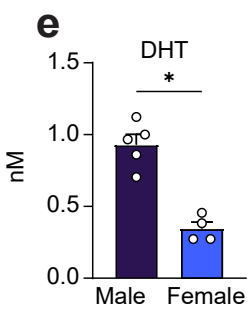

Extended Data Fig. 1 | Greater bacterial growth and skin damage in male mice compared to female mice. a,**b**, Male and female C57BL/6 wild-type (WT) mice were epicutaneously infected for 4 days with 1×10^6 colony forming units (CFUs) of a bioluminescent strain of MRSA SAP430 (MRSA::*lux*). Bioluminescence quantified over time. *In vivo* bioluminescence images (**a**) and diseases scores (**b**) quantified on Day 4. **c**, Transepidermal water loss (TEWL), a measure of skin barrier damage, quantified by Vapometer on Day 0 and Day 4. **d**,**e**, Testosterone (**d**) and dihydrotestosterone (DHT) (**e**) quantified from the skin secretions of male and female mice by hormone immunoassay. Means ± SEM are plotted ($n = 5$/group). (**b**) $^*p < 0.05$ by two-sided Kolmogorov-Smirnov Test. (**c**) $^{**}p < 0.001$ by two-way ANOVA (two-sided) with Sidak's correction for multiple comparisons. (**d**,**e**) $^*p < 0.05$ $^{**}p < 0.01$ by Mann-Whitney *U*-test (two-sided).

https://doi.org/10.1038/s41564-026-02261-2

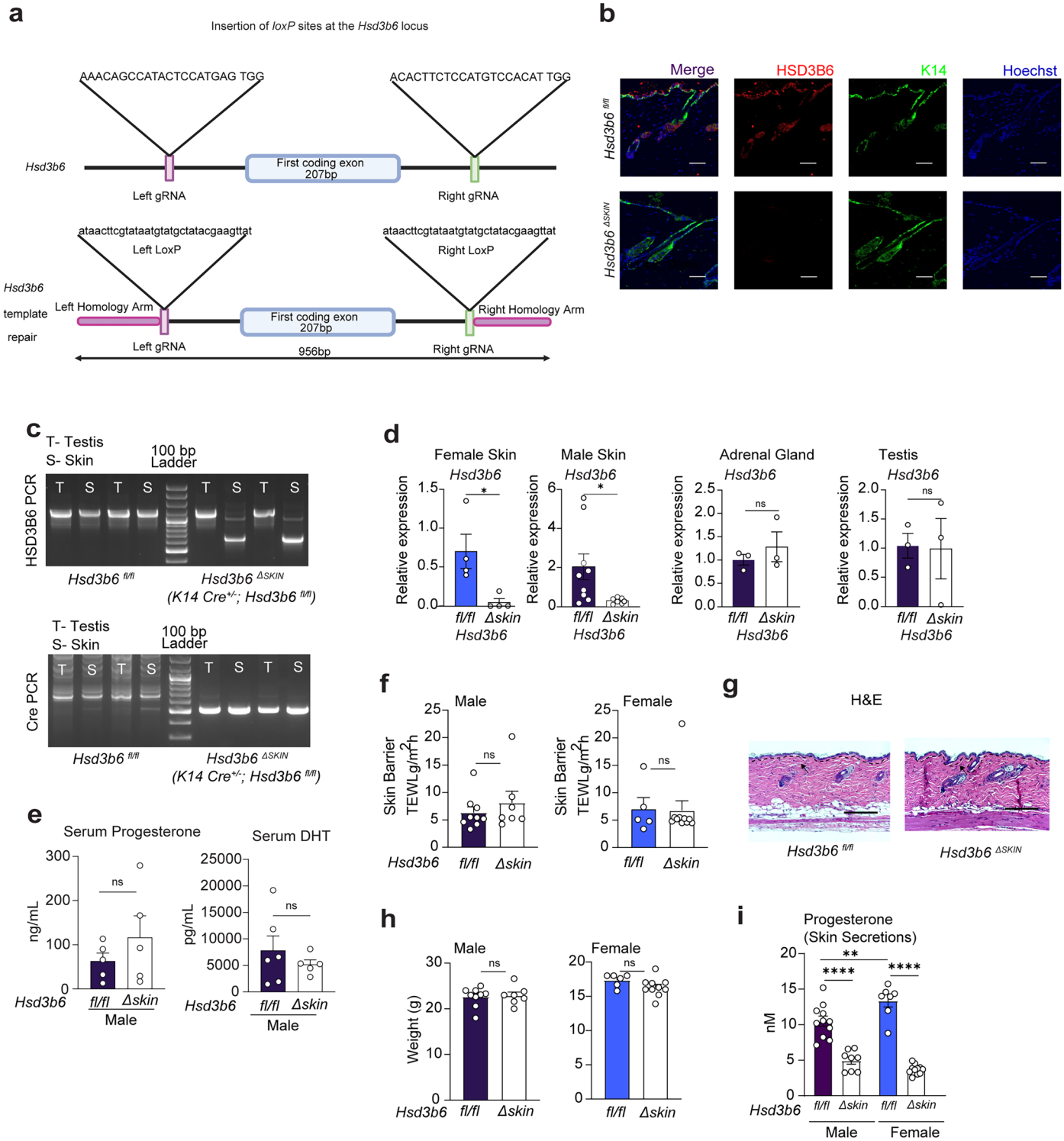

Extended Data Fig. 2 | Generation and validation of *Hsd3b6*$^{\Delta skin}$ mice by CRISPR/Cas9 genomic tar-geting and baseline analysis of the *Hsd3b6*$^{\Delta skin}$ mice compared to control. a, Schematic diagram of CRISPR/Cas9-mediated gene insertion of *loxP* sites flanking the first coding exon of the *Hsd3b6* locus. *Hsd3b6*$^{fl/fl}$ mice crossed with K14-Cre$^{+/-}$ mice to generate *Hsd3b6*$^{\Delta skin}$ mice (K14-Cre$^{+/-}$; *Hsd3b6*$^{fl/fl}$). **b**, Immunofluorescence staining of HSD3B6 expression in *Hsd3b6*$^{fl/fl}$ *and Hsd3b6*$^{\Delta skin}$ mice skin. Scale bar 50 µM. **c**, Genomic confirmation of *loxP* mediated deletion of *Hsd3b6* in the K14Cre$^{+/-}$ mice in the skin, with PCR of testicular samplings demonstrating tissue specificity. **d**, qRT-PCR for *Hsd3b6* expression *Hsd3b6*$^{fl/fl}$ ($n = 4$) and *Hsd3b6*$^{\Delta skin}$ ($n = 4$) in the female skin and *Hsd3b6*$^{fl/fl}$ ($n = 9$) and *Hsd3b6*$^{\Delta skin}$ ($n = 7$) in the male skin, *Hsd3b6*$^{fl/fl}$ ($n = 3$) and *Hsd3b6*$^{\Delta skin}$ ($n = 3$) in testis, and *Hsd3b6*$^{fl/fl}$ ($n = 3$) and *Hsd3b6*$^{\Delta skin}$ ($n = 3$) in the adrenal gland normalized to Rplp0 expression. **e**, Serum progesterone in male *Hsd3b6*$^{fl/fl}$ ($n = 5$) and *Hsd3b6*$^{\Delta skin}$ ($n = 5$) and DHT in male *Hsd3b6*$^{fl/fl}$ ($n = 6$) and *Hsd3b6*$^{\Delta skin}$ ($n = 5$) quantified by hormone immunoassay. **f**, Transepidermal water loss (TEWL) of male *Hsd3b6*$^{fl/fl}$ ($n = 9$) and *Hsd3b6*$^{\Delta skin}$ ($n = 7$) and female *Hsd3b6*$^{fl/fl}$ ($n = 5$) and *Hsd3b6*$^{\Delta skin}$ ($n = 10$) mice measured by Vapometer device as a metric of barrier integrity. **g**, Hematoxylin and eosin staining of *Hsd3b6*$^{fl/fl}$ and *Hsd3b6*$^{\Delta skin}$ skin. Scale bar 220 µM. **h**, Weight measurements of male *Hsd3b6*$^{fl/fl}$ ($n = 9$) and *Hsd3b6*$^{\Delta skin}$ ($n = 7$) and female *Hsd3b6*$^{fl/fl}$ ($n = 6$) and *Hsd3b6*$^{\Delta skin}$ ($n = 10$) mice. **i**, Progesterone quantified from the skin secretions of male *Hsd3b6*$^{fl/fl}$ ($n = 11$) and *Hsd3b6*$^{\Delta skin}$ ($n = 8$) and female *Hsd3b6*$^{fl/fl}$ ($n = 7$) and *Hsd3b6*$^{\Delta skin}$ ($n = 11$) age-matched mice at 7 weeks by hormone immunoassay. Means ± SEM (error bars) are plotted. (d) $^{*}p < 0.05$, $^{***}p < 0.001$, ns, not significant by one-way ANOVA. (e-f,h) ns by Mann-Whitney U-test (two-sided). (i) $^{**}p < 0.01$, $^{****}p < 0.0001$ by Kruskal-Wallis test with correction for false discovery (two-sided).

https://doi.org/10.1038/s41564-026-02261-2

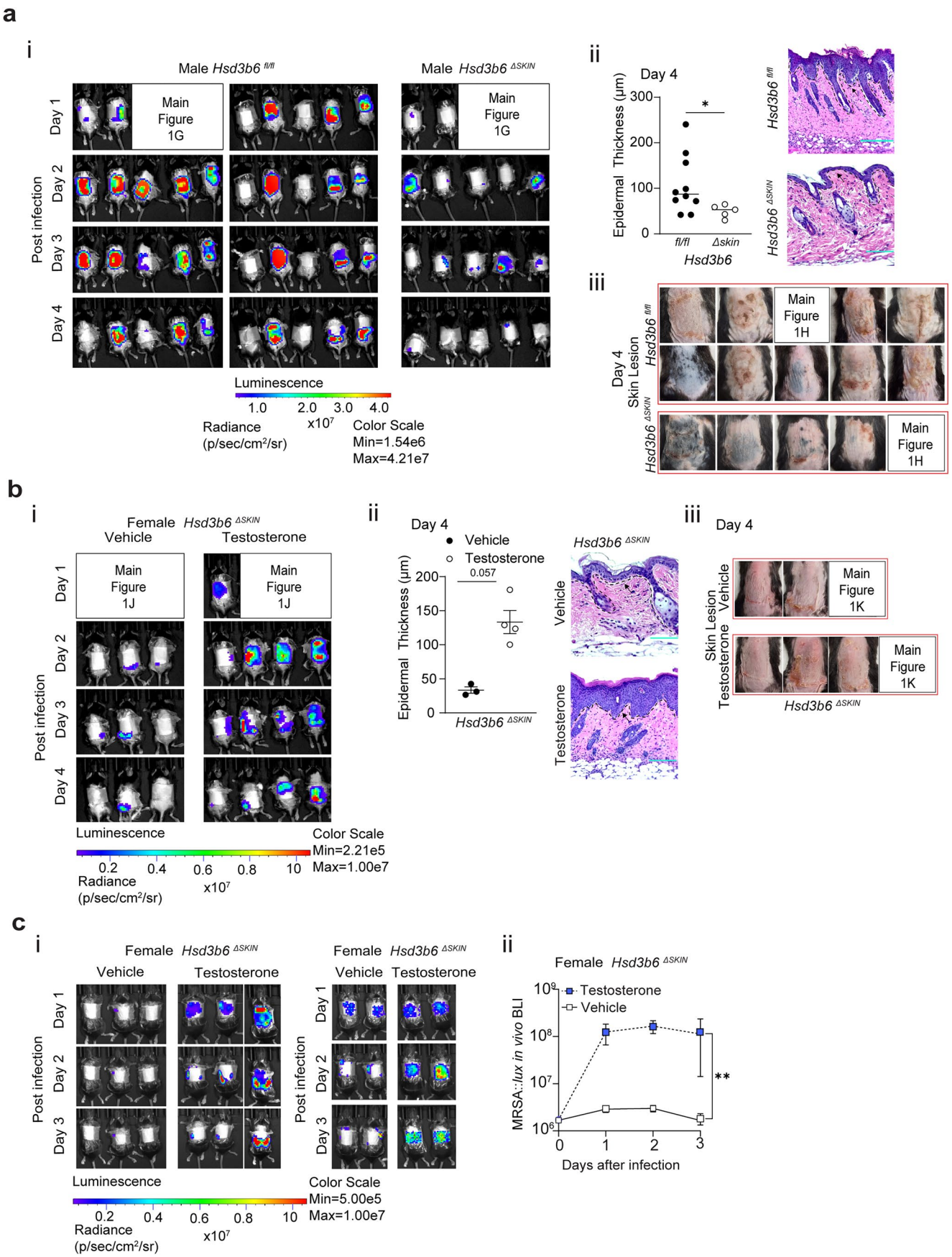

Extended Data Fig. 3 | See next page for caption.

https://doi.org/10.1038/s41564-026-02261-2

Extended Data Fig. 3 | *Hsd3b6*$^{\Delta skin}$ mice are resistant to skin infection with *S. aureus* and topical testosterone increases *S. aureus* infection. Images related to Fig. 1g and j. **a**, Male *Hsd3b6*$^{fl/fl}$ ($n = 10$) and *Hsd3b6*$^{\Delta skin}$ ($n = 5$) mice epicutaneously infected for 4 days with 1×10^6 CFUs of MRSA SAP430 (MRSA::*lux*). (i) Images related to Fig. 1g. (ii) Representative histology (H&E stain) and mean epidermal thickness (μm) ± SEM. Scale bars: 220 μm. *$p < 0.05$, by Mann-Whitney *U*-test (two-sided). Means ± SEM are plotted. (iii) Representative images showing skin lesions on day 4 post-infection. **b**, Female *Hsd3b6*$^{\Delta skin}$ mice were epicutaneously challenged with 1×10^6 CFUs with bioluminescent MRSA SAP430 (MRSA::*lux*) for 4 days with or without testosterone (vehicle, $n = 3$; testosterone $n = 4$). (i) Images related to Fig. 1j. (ii) Representative histology (H&E stain) and mean epidermal thickness (μm) ± SEM. Scale bars: 220 μm. ns, $p \geq 0.057$ by Mann-Whitney *U*-test (two-sided). Means ± SEM are plotted. (iii) Representative images showing skin lesions on day 4 post-infection. **c**, Repeat of Female *Hsd3b6*$^{\Delta skin}$ mice were epicutaneously challenged with 1×10^6 CFUs with bioluminescent MRSA SAP430 (MRSA::*lux*) for 3 days with or without testosterone (vehicle, $n = 5$; testosterone, $n = 5$). Means ± SEM (error bars) are plotted. **$p < 0.001$ by two-way ANOVA. (i) Representative bioluminescence imaging (BLI) of mice at days 1, 2, and 3 post-infections. (ii) Quantification of infection progression over days.

https://doi.org/10.1038/s41564-026-02261-2

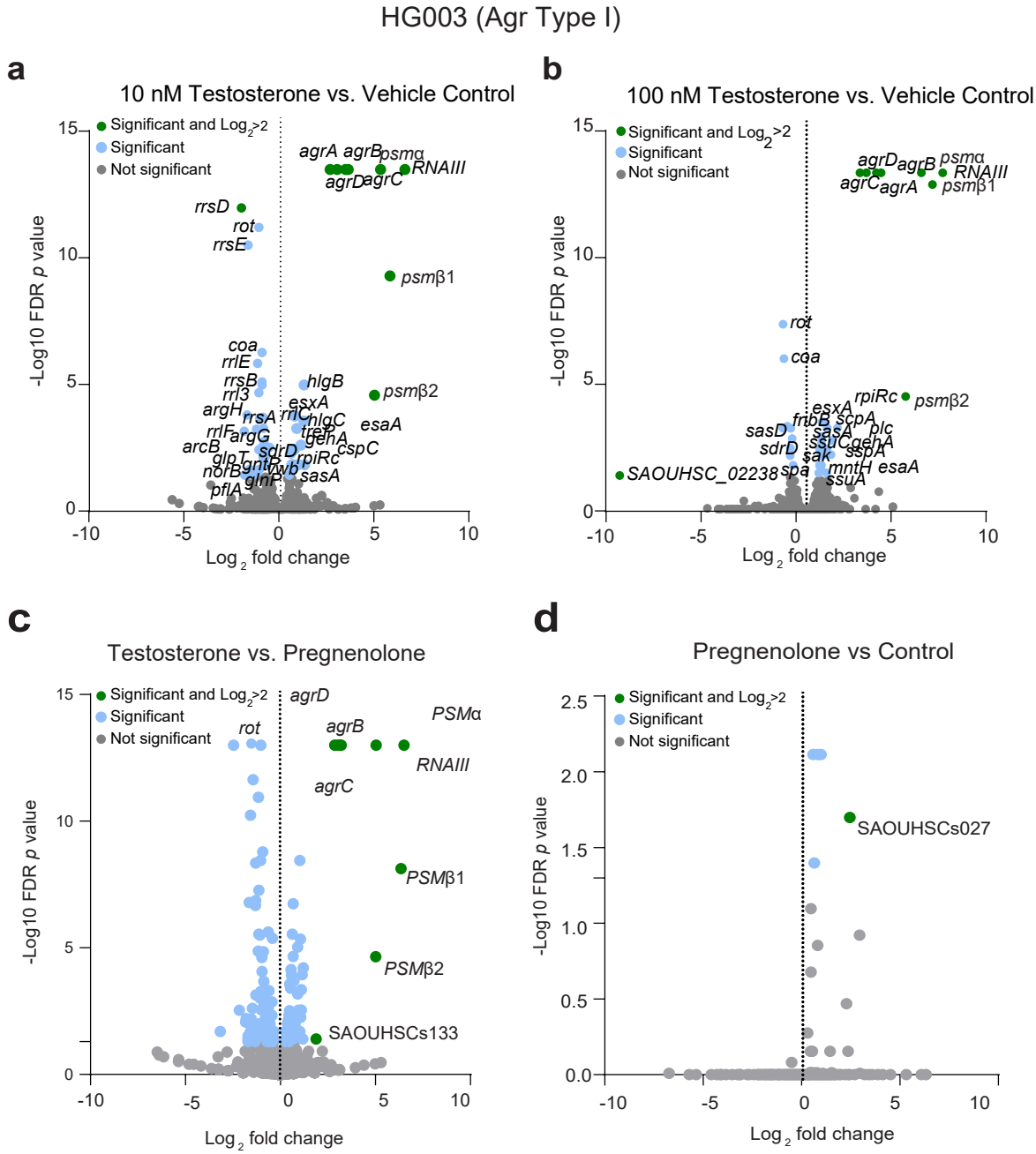

Extended Data Fig. 4 | Testosterone stimulates quorum sensing readouts in *S. aureus*, but pregnenolone does not activate quorum sensing. **a**-**d**, Transcriptomics (RNA-seq) of HG003 strain of *S. aureus* treated through the early-log phase (OD_{600} 0.4) with 10 nM or 100 nM testosterone, 10 nM pregnenolone, or vehicle alone. Differential gene expression was analysed using DESeq2 (two-sided Wald test) with Benjamini-Hochberg correction for multiple comparisons (FDR). **a**, Volcano plot demonstrating genes fold change in expression in testosterone transcriptome compared to vehicle treated *S. aureus*, ($n = 3$) as shown in Fig. 2a. Here, additional significant genes with lower fold-change are labelled. **b**, Volcano plot demonstrating change in expression with 100 nM of testosterone transcriptome compared to vehicle treated *S. aureus*, ($n = 3$). **c**, Volcano plot demonstrating change in expression with 10 nM of testosterone transcriptome compared to pregnenolone treated *S. aureus*, ($n = 3$). **d**, Volcano plot comparing the transcriptome of *S. aureus* treated with pregnenolone compared to vehicle control ($n = 3$).

https://doi.org/10.1038/s41564-026-02261-2

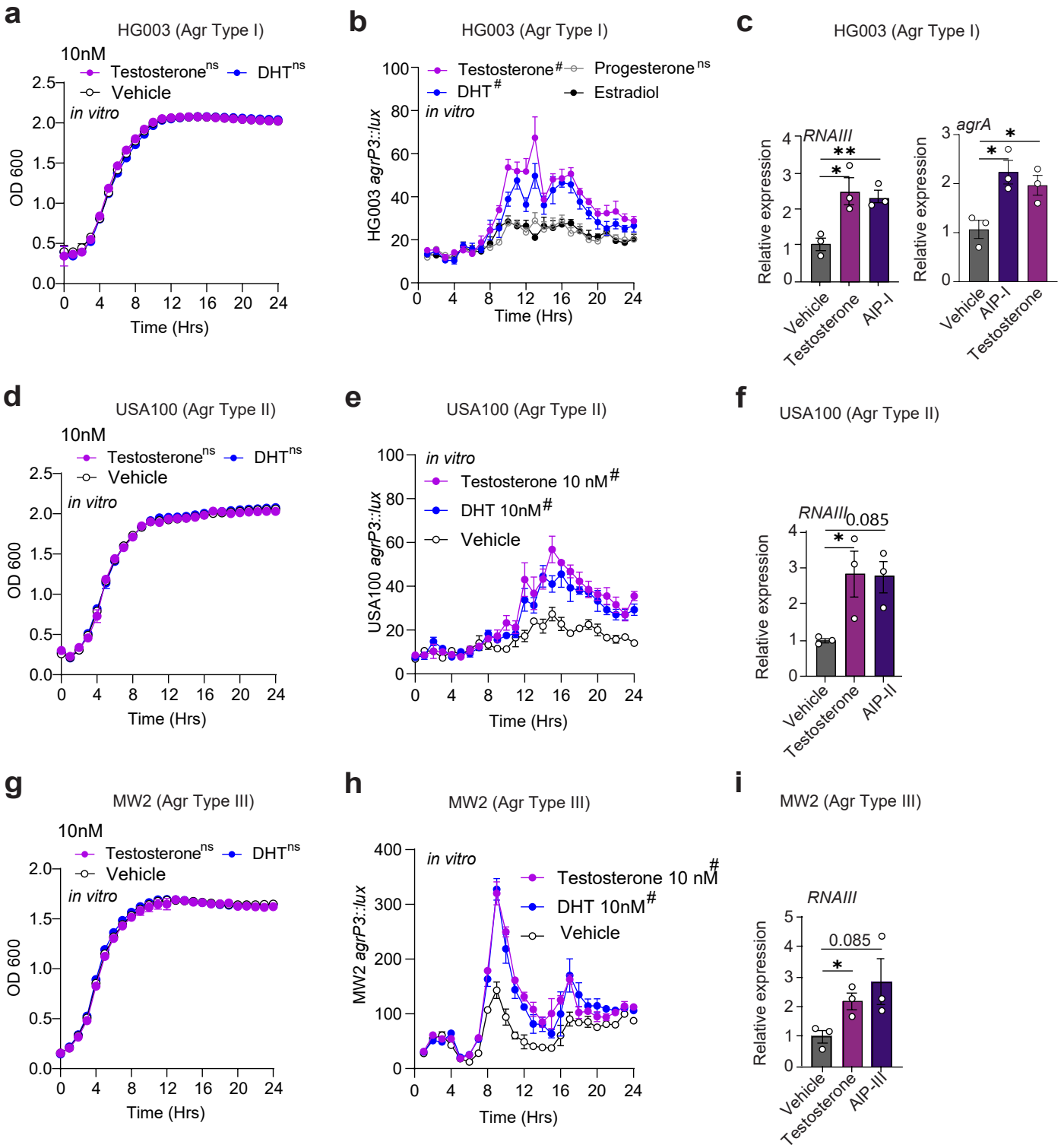

Extended Data Fig. 5 | See next page for caption.

https://doi.org/10.1038/s41564-026-02261-2

Extended Data Fig. 5 | Testosterone and DHT activate quorum sensing in *S. aureus* without affecting growth, and other hormone classes have no effect on quorum sensing. a, Growth curve of HG003 (agr Type I) treated with 10 nM testosterone or DHT. ns by two-way ANOVA compared to Vehicle. **b**, Bioluminescence of agr-P3 reporter (HG003agrP3::lux) treated with testosterone, DHT, progesterone, or estradiol. #p < 0.0001 or ns by two-way ANOVA com-pared to estradiol. **c**, qRT-PCR of S. aureus HG003 strain (agr Type I) treated with 10 nM testos-terone or AIP-I (n = 3) till early-growth phase (OD600 0.6). Expression of target genes RNAIII and agrA normalized to gyrA expression. **p < 0.001, *p < 0.05by two-tailed unpaired t-test. **d**, Growth curve of USA100 (agr Type II) treated with 10 nM testosterone or DHT. ns, not significant by two-way ANOVA compared to vehicle. **e**, In vitro bioluminescence of USA100 (USA100 agrP3::lux) treated with 10 nM of testosterone or DHT (n = 3). #p < 0.0001, by two-way ANOVA compared to vehicle control. **f**, qRT-PCR of USA100 treated with 10 nM testosterone or respective AIP (n = 3) through mid-log phase (OD600 0.6). Expression of target genes RNAIII normalized to gyrA expres-sion. Means ± SEM (error bars) are plotted. *p < 0.05by two-tailed unpaired t-test. **g**, Growth curve of MW2 (agr Type III) treated with 10 nM testosterone or DHT. ns,not significant by two-way ANOVA compared to Vehicle. **h**, In vitro bioluminescence of MW2 (MW2 agrP3::lux) treated with 10 nM of testosterone or DHT (n = 3). #p < 0.0001, by two-way ANOVA compared to vehicle control. **i**, qRT-PCR of MW2 treated with 10 nM testosterone or respective AIP (n = 3) through mid-log phase (OD600 0.6). Expression of target genes RNAIII normalized to gyrA expression. Means ± SEM (error bars) are plotted. *p > 0.05, ns, not significant by two-tailed unpaired t-test.

https://doi.org/10.1038/s41564-026-02261-2

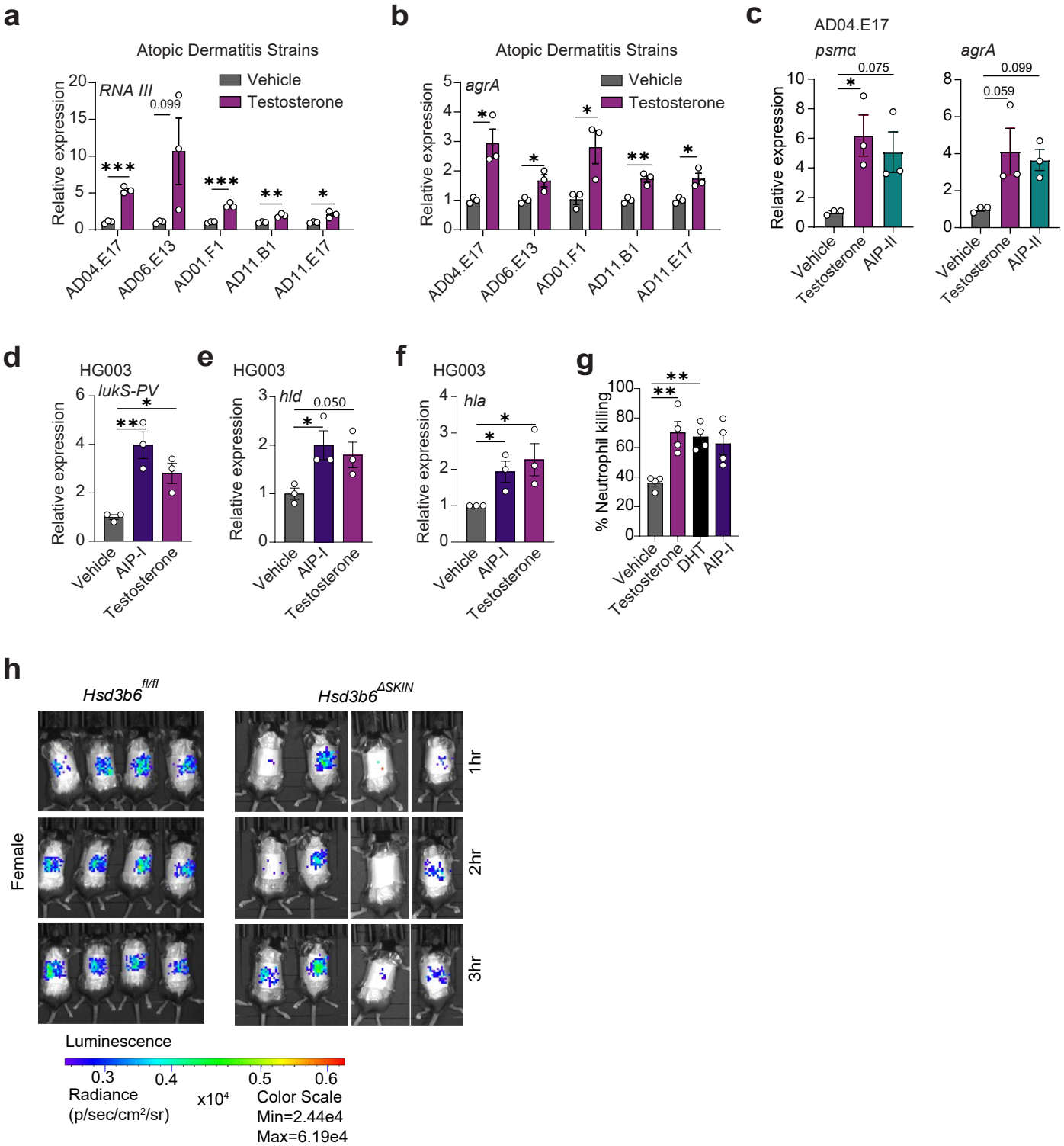

Extended Data Fig. 6 | Testosterone stimulates the expression of virulence factors across strains of *S. aureus* and *in vivo* quorum sensing bioluminescence of female *Hsd3b6*$^{\Delta skin}$ compared to controls. a,b, qRT-PCR of strains of *S. aureus* obtained from patients with atopic dermatitis[46] and treated with 10 nM of testosterone to the mid-exponential growth ($n = 3$). Expression of target gene *RNAIII* (**a**), and *agrA* (**b**), normalized to housekeeping gene *gyrA* expression. Means ± SEM (error bars) are plotted. $^{**}p < 0.001$, $^{*}p < 0.05$; $p > 0.05$ ns, not significant by two-tailed unpaired *t*-test. **c**, qRT-PCR of AD04.E7 treated with 10 nM testosterone or AIP-II ($n = 3$) till late-exponential growth (OD_{600} 1.0). Expression of target genes, *psmα*, and *agrA* normalized to *gyrA* expression. Means ± SEM (error bars) are plotted. $^{*}p < 0.05$, $p > 0.05$ ns, not significant by one-way ANOVA. **d-f**, qRT-PCR of *S. aureus agr* Type I strain HG003 treated with 10 nM testosterone or AIP-I ($n = 3$) till late-exponential growth (OD_{600} 1.0). Expression of target genes, *lukS-PV*, *hld*, and *hla* normalized to *gyrA* expression. Means ± SEM (error bars) are plotted. $^{*}p < 0.05$; $^{**}p < 0.01$ by two-tailed unpaired *t*-test. **g**, Percentage of bacterially-induced neutrophil killing from *S. aureus* treated with and without 10 nM testosterone, DHT or AIP-I. $n = 4$ human donors, 2 male and 2 female. Means ± SEM (error bars) are plotted. $^{**}p < 0.01$, by one-way ANOVA. **h**, *In vivo* analysis of *agr*-P3 reporter. Female *Hsd3b6*$^{fl/fl}$ and *Hsd3b6*$^{\Delta skin}$ mice were epicutaneously infected with 1×10^{6} CFUs of the CA-MRSA-*agr-P3lux* and bioluminescence quantified over time in Fig. 2j.

https://doi.org/10.1038/s41564-026-02261-2

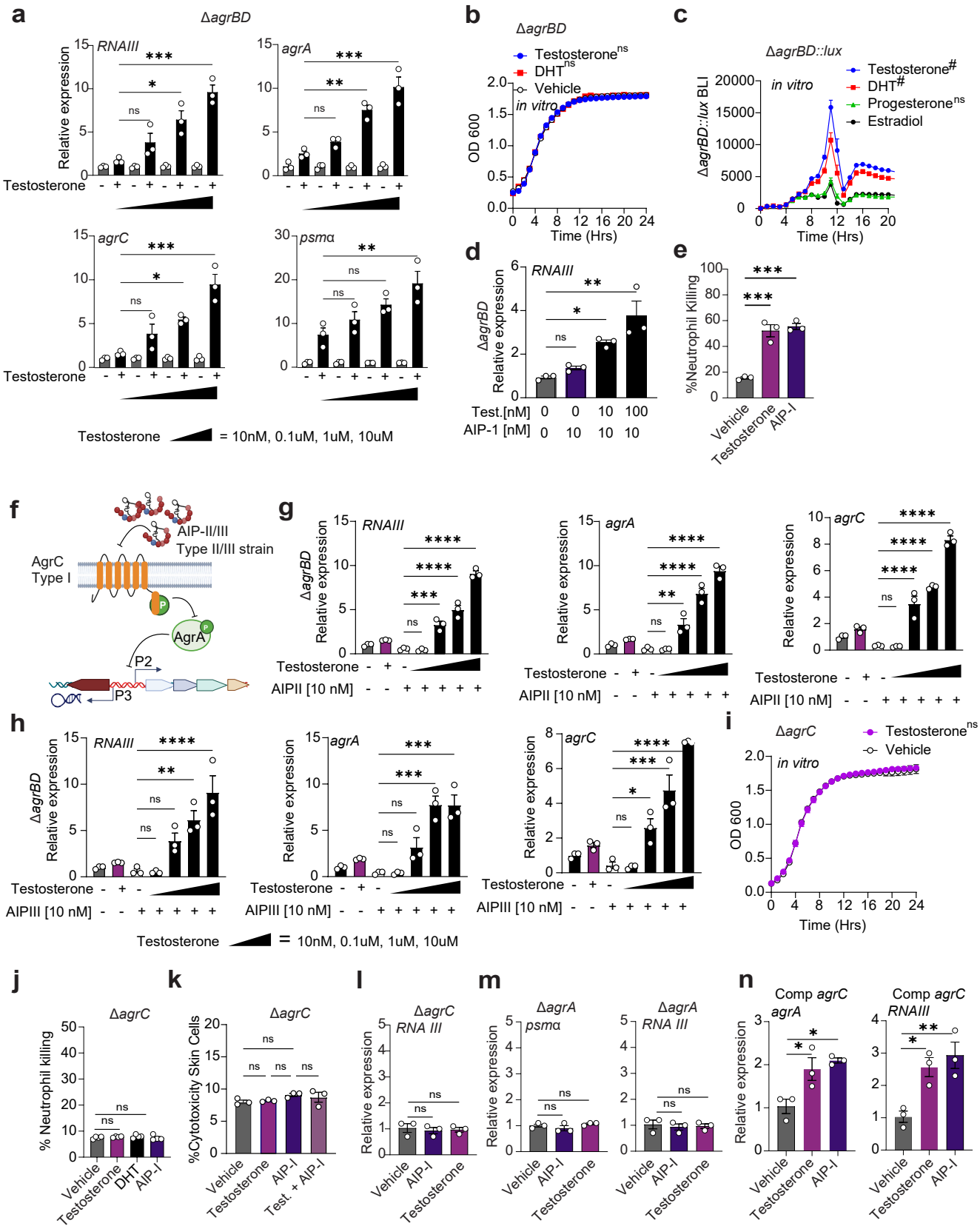

Extended Data Fig. 7 | See next page for caption.

https://doi.org/10.1038/s41564-026-02261-2

Extended Data Fig. 7 | Testosterone stimulates *S. aureus agr* quorum sensing in a dose-dependent man-ner and requires AgrC and AgrA. a, Biosynthetic mutant Δ*agrBD* treated with increasing concentrations of testosterone. *RNAIII*, *agrA*, *agrC*, and *psmα* quantified by qRT-PCR ($n = 3$).Means ± SEM (error bars) are plotted. *$p < 0.05$; ***$p < 0.001$, ns, not significant by one-way ANOVA with Tukey's post-hoc test (two-sided), adjusted for multiple comparisons. **b**, Growth curves of Δ*agrBD* treated with 10 nM testosterone, DHT or vehicle ($n = 3$), no significant differences from vehicle by two-way ANOVA. Means ± SEM (error bars) are plotted. **c**, Δ*agrBD::lux* treated with 10 nM testosterone, DHT, progesterone, or estradiol ($n = 3$). Bioluminescence was measured. Means ± SEM (error bars) are plotted. **d**, *RNAIII* expression in Δ*agrBD* treated with 10 nM AIP-I and 10 or 100 nM testosterone ($n = 3$) was quantified. **e**, Neutrophil killing induced by Δ*agrBD* treated with 10 nM testosterone, AIP-I, or vehicle was measured ($n = 3$ from a single donor). Means ± SEM are plotted. (**c**-**e**) *$p < 0.05$; **$p < 0.01$, ***$p < 0.001$, ****$p < 0.0001$, ns, not significant by one-way ANOVA (two-sided). (**c**) $^{\#}p < 0.0001$ and ns by two-way ANOVA (two-sided). versus estradiol. **f**, Schematic showing inhibition of AgrC signaling by non-cognate AIPs. **g,h**, Δ*agrBD* strains were treated with AIP-II (**g**) or AIP-III (**h**) alone or with increasing concentrations of testosterone (10nM–10 μM).*RNAIII*, *agrA*, and *agrC* were quantified ($n = 3$). Means ± SEM (error bars) are plotted. *$p < 0.05$, **$p < 0.01$; ***$p < 0.001$, ****$p < 0.0001$, ns by one-way ANOVA. **i**, Growth curve of Δ*agrC* treated with 10 nM testosterone showed no significant difference from vehicle ($n = 3$) by two-way ANOVA. Means ± SEM (error bars) are plotted. **j,k**, Neutrophil killing ($n = 3$ replicates of RBCs from a single donor) (**j**) and skin cell cytotoxicity ($n = 3$) (k) analysed in Δ*agrC* treated with 10 nM testosterone, DHT, AIP-I, or combinations. ns by one-way ANOVA. Means ± SEM (error bars) are plotted. **l,m**, Δ*agrC* (**l**) and Δ*agrA* (m) mutants were treated with 10 nM testosterone, AIP-I, or vehicle, ($n = 3$) and *psmα* and *RNAIII* were quantified. Means ± SEM (error bars) are plotted. ns, not significant by one-way ANOVA. **n**, Δ*agrC* mutant strain complemented (Comp) with AgrC on a plasmid treated with 10 nM testosterone, AIP-I, or vehicle ($n = 3$) and *agrA* and *RNAIII* were quantified. Means ± SEM (error bars) are plotted. *$p < 0.05$ by one-way ANOVA. Panel **f** created in BioRender; Harris, T. https://biorender.com/dzfdpzh (2025).

https://doi.org/10.1038/s41564-026-02261-2

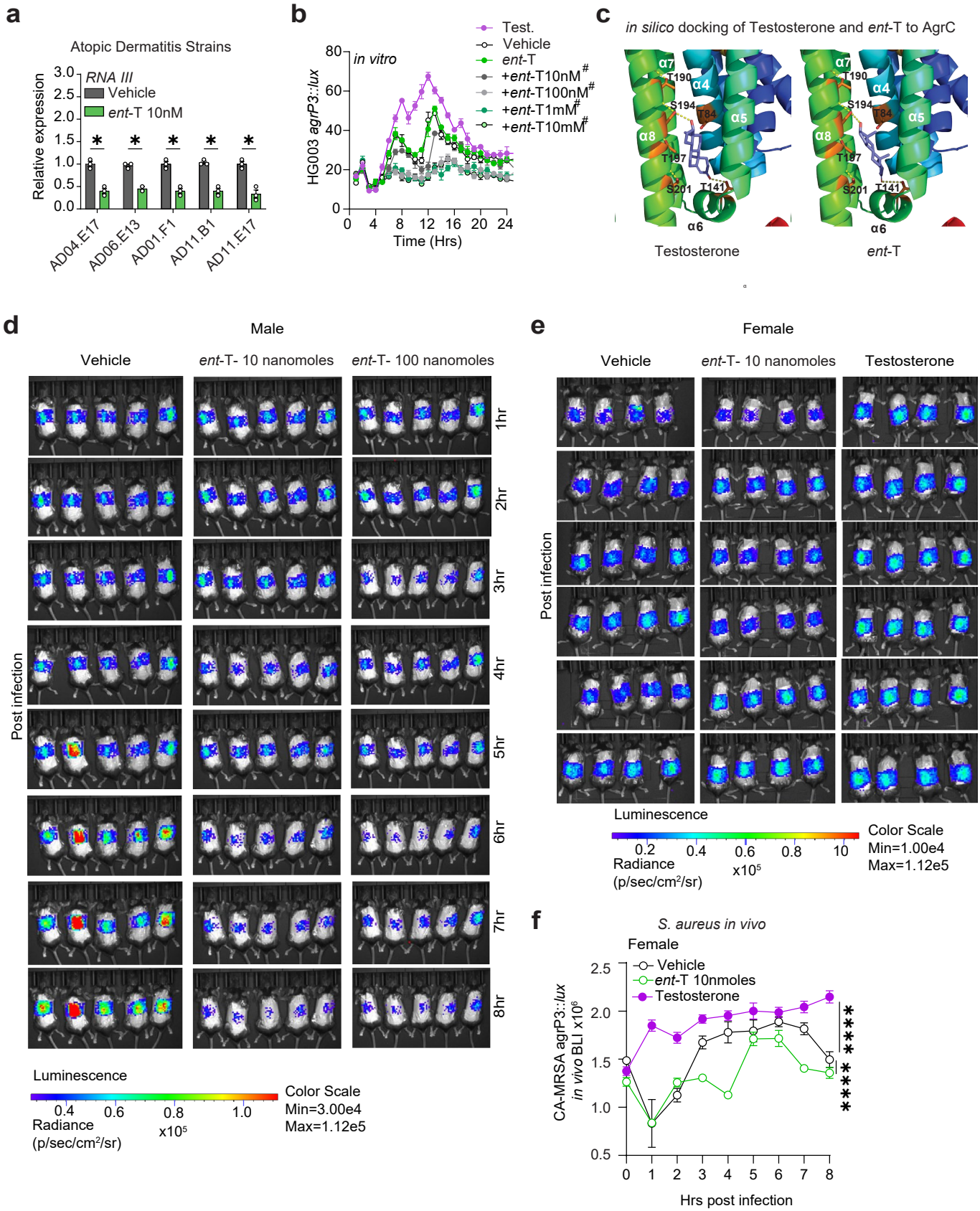

Extended Data Fig. 8 | See next page for caption.

https://doi.org/10.1038/s41564-026-02261-2

Extended Data Fig. 8 | *Enantiomer*-testosterone (*ent*-T) inhibits the expression of RNA III in atopic dermatitis strains of *S. aureus* and also inhibits *S. aureus* quorum sensing in male and female mice *in vivo*. **a**, qRT-PCR of strains of *S. aureus* obtained from patients with atopic dermatitis[46] and treated with 10 nM or *ent*-T, a stereoisomer of testosterone ($n = 3$). Expression of target gene *RNAIII* normalized to housekeeping gene *gyrA* expression. Means ± SEM (error bars) are plotted.*$p < 0.05$ by two-tailed paired *t*-test. **b**, Bioluminescence of *agr*-P3 reporter (HG003*agrP3::lux*) treated with testosterone, *ent*-T or testosterone with escalating amounts of *ent*-T at the same time as testosterone. $^{\#}p < 0.0001$ or ns by two-way ANOVA compared to testosterone alone. **c**, *In silico* analysis with testosterone (left) and *ent*-T (right) bound to a hydrophobic pocket of AgrC bound by the polar residues T141, T197, and S201. Testosterone (left) is predicted to form stable hydrogen bonds with S194 and T190. *Ent*-T (right)is predicted to bind to the same hydrophobic pocket, but without the equivalent stability of hydrogen-bond interactions. **d**, Bioluminescence images of Fig. 5g, male wild-type mice epicutaneously infected with 1×10^6 CFUs CA-MRSA-*agr*-P3 *S. aureus* reporter treated with *ent*-T or vehicle. **e**, Bioluminescence images of female wild-type mice epicutaneously infected with 1×10^6 CFUs CA-MRSA-*agr*-P3 *S. aureus* reporter treated with testosterone, *ent*-T, or vehicle, and **f**, Bioluminescence quantified over time ****$p < 0.0001$ by two-way ANOVA with comparisons shown. Means ± SEM (error bars) are plotted.

nature portfolio

Corresponding author(s): Tamia A. Harris-Tryon

Last updated by author(s): Dec 15, 2025

Reporting Summary

Nature Portfolio wishes to improve the reproducibility of the work that we publish. This form provides structure for consistency and transparency in reporting. For further information on Nature Portfolio policies, see our Editorial Policies and the Editorial Policy Checklist.

Statistics

For all statistical analyses, confirm that the following items are present in the figure legend, table legend, main text, or Methods section.

n/a	Confirmed	
☐	☒	The exact sample size (*n*) for each experimental group/condition, given as a discrete number and unit of measurement
☒	☐	A statement on whether measurements were taken from distinct samples or whether the same sample was measured repeatedly
☐	☒	The statistical test(s) used AND whether they are one- or two-sided *Only common tests should be described solely by name; describe more complex techniques in the Methods section.*
☒	☐	A description of all covariates tested
☐	☒	A description of any assumptions or corrections, such as tests of normality and adjustment for multiple comparisons
☐	☒	A full description of the statistical parameters including central tendency (e.g. means) or other basic estimates (e.g. regression coefficient) AND variation (e.g. standard deviation) or associated estimates of uncertainty (e.g. confidence intervals)
☐	☒	For null hypothesis testing, the test statistic (e.g. *F*, *t*, *r*) with confidence intervals, effect sizes, degrees of freedom and *P* value noted *Give P values as exact values whenever suitable.*
☒	☐	For Bayesian analysis, information on the choice of priors and Markov chain Monte Carlo settings
☒	☐	For hierarchical and complex designs, identification of the appropriate level for tests and full reporting of outcomes
☒	☐	Estimates of effect sizes (e.g. Cohen's *d*, Pearson's *r*), indicating how they were calculated

Our web collection on statistics for biologists contains articles on many of the points above.

Software and code

Policy information about availability of computer code

Data collection	No unpublished software was used to collect data.
Data analysis	All approaches to statistical analyses are detailed in the manuscript. GraphPad Prism software (Version 10.0.1) was used throughout, with the exception of the bioluminescences data which was analyzed with living image software (Xenogen, Alameda, CA).

For manuscripts utilizing custom algorithms or software that are central to the research but not yet described in published literature, software must be made available to editors and reviewers. We strongly encourage code deposition in a community repository (e.g. GitHub). See the Nature Portfolio guidelines for submitting code & software for further information.

Data

Policy information about availability of data

All manuscripts must include a data availability statement. This statement should provide the following information, where applicable:

- Accession codes, unique identifiers, or web links for publicly available datasets
- A description of any restrictions on data availability
- For clinical datasets or third party data, please ensure that the statement adheres to our policy

Sequencing data have been submitted to the National Center for Biotechnology Information Sequence Read Archive under BioProject accession number PRJNA1071176.

Research involving human participants, their data, or biological material

Policy information about studies with human participants or human data. See also policy information about sex, gender (identity/presentation), and sexual orientation and race, ethnicity and racism.

Reporting on sex and gender	Findings apply to all sexes. Sex was considered in study design. Sex and gender for human subjects was determined based on self reporting. All data presented in the manuscript is disaggregated by sex and gender. Consent was obtained for sharing individual level details. Sex based analysis was performed on human data as sex was central to question being asked.
Reporting on race, ethnicity, or other socially relevant groupings	Race, ethnicity, and socially relevant groupings were not considered in study design.
Population characteristics	Participants were healthy with no relevant diagnoses. One participant was a Hispanic White male, aged 28. One participant was an Non-Hispanic Asian female aged 26 years.
Recruitment	Participants were recruited via word-of-mouth. Data was collected in a private setting at the University of Texas Southwestern Medical Center. Samples were collected between June 2024 and August 2024 Recruitment occurred from January 2024 to June 2024.
Ethics oversight	All experiments involving humans were approved by the IRB of the University of Texas Southwestern Medical Center IRB. (STU 2019-0145)

Note that full information on the approval of the study protocol must also be provided in the manuscript.

Field-specific reporting

Please select the one below that is the best fit for your research. If you are not sure, read the appropriate sections before making your selection.

☒ Life sciences ☐ Behavioural & social sciences ☐ Ecological, evolutionary & environmental sciences

For a reference copy of the document with all sections, see nature.com/documents/nr-reporting-summary-flat.pdf

Life sciences study design

All studies must disclose on these points even when the disclosure is negative.

Sample size	Invitro studies includes technical replicates n=3 considered for bacterial cultures and HaCaT cell lysis assays per treatment group, three technical replicates per biological replicate considered for whole blood and neutrophil lysis assays. The sample size is consistent with similar in vitro studies that typically use this number of replicates to achieve statistically significant results and ensure robust statistical analysis. For mice studies, the sample size (ranging from 4-10/group) was determined based on a power calculation to detect a significant difference between groups with a power of 80% to ensure sufficient statistical power.
Data exclusions	Data exclusion for in vitro and in vivo studies was not performed as all collected data met the experimental criteria, with no outliers or irregular data points identified. All measurements were valid, and experimental procedures were followed according to protocol, ensuring consistency and reliability. To maintain transparency and reproducibility, all data points were included for a comprehensive analysis, ensuring that all experimental outcomes were presented without selection bias. For human data,each data point represents and average of individual measurements taken. A dual sided Grubb's test was performed once for each data point, and a single outlier was excluded if $p < 0.05$. `
Replication	For the experiments with whole blood and neutrophils cell lysis 3 independent technical replicates from four biologically distinct donors (two male and two female donors) were performed and 3 biological technical replicates performed for HaCaT cell lysis and in vitro bacterial treatment groups were used for all statistical analyses in biological experiments to ensure the reproducibility and consistency of the results.
Randomization	Bacteria: Randomization was not performed as bacterial cultures were derived from a genetically identical clonal population, ensuring uniformity across all experimental groups. Additionally, bacterial samples were assigned to treatment groups based on predefined growth phase criteria (stationary phase) to maintain consistency across experimental conditions. Mouse: Randomization was not performed. Mice were assigned to experimental groups based on predefined criteria (e.g., age-matched, sex, genotype) to ensure consistency across conditions. Also, mice used were housed under controlled, uniform environmental conditions, minimizing variability between groups.
Blinding	Whenever possible, data analysis was completed in a blinded manner. For clinical studies, participants were allocated to group via sex, blinding of the researcher collecting samples was not possible. All steps downstream of collection and immediate processing were completed by an analytical chemist who was blinded to the experimental conditions. Disease scoring of skin infection after bacterial treatment was conducted in a blinded manner, with the outcome assessors unaware of the experimental group assignments to minimize observer bias. Blinding was also performed within a subset of experiments to reduce bias. In these experiments, mice were assigned to experimental groups without knowledge of their genotype allocation (Hsd3b6fl/fl and Hsd3b6Δskin) ensuring unbiased treatment application and bioluminescent measurements.

Reporting for specific materials, systems and methods

We require information from authors about some types of materials, experimental systems and methods used in many studies. Here, indicate whether each material, system or method listed is relevant to your study. If you are not sure if a list item applies to your research, read the appropriate section before selecting a response.

Materials & experimental systems

n/a	Involved in the study
☐	☒ Antibodies
☐	☒ Eukaryotic cell lines
☒	☐ Palaeontology and archaeology
☐	☒ Animals and other organisms
☒	☐ Clinical data
☒	☐ Dual use research of concern
☒	☐ Plants

Methods

n/a	Involved in the study
☒	☐ ChIP-seq
☒	☐ Flow cytometry
☒	☐ MRI-based neuroimaging

Antibodies

Antibodies used: anti-HSD3B6 (2.5 µg/mL; Biorbyt; orb592071), anti- cytokeratin-14 (1 µg/mL; Santa Cruz Biotechnology; sc-53253), Donkey anti-rabbit alexa-fluor-647 (2 µg/mL; Jackson Immuno; 711-605-152), Donkey anti-mouse alexa-fluor-594 (2 µg/mL; Thermofisher Scientific; A-21203).

Validation:
Primary antibodies-
anti-HSD3B6- RRID:AB_3665641, validated by manufacturer for use in western blot, host species mouse.
anti-cytokeratin-14- RRID:AB_2134820, validated by manufacturer for western blot, immunofluorescence,and immunohistochemistry, host species mouse.
Secondary antibodies-
Donkey anti-rabbit alexa-fluor-647- RRID:AB_2492288, validated by manufacturer for: immunofluorescence, immunocytochemistry, and western blot, host species donkey.
Donkey anti-mouse alexa-fluor-594- RRID:AB_2535789, validated by manufacturer for immunocytochemistry and immunohistochemistry, host species donkey.

Eukaryotic cell lines

Policy information about cell lines and Sex and Gender in Research

Cell line source(s): HaCaT keratinocytes cell line from histologically normal skin from a 62 year old Caucasian male.

Authentication: Cells were authenticated upon purchase from the manufacturer.

Mycoplasma contamination: This cell line has tested negative for mycoplasma contamination.

Commonly misidentified lines (See ICLAC register): This study does not include any commonly misidentified cell lines.

Animals and other research organisms

Policy information about studies involving animals; ARRIVE guidelines recommended for reporting animal research, and Sex and Gender in Research

Laboratory animals: Conventionally raised C57BL6/J male and female mice aged 6-9 weeks old mice were purchased from the Jackson Laboratory. C57BL6/J wild-type, K14Cre+/-, and Hsd3b6fl/fl mice were bred and maintained in the specific pathogen-free (SPF) barrier facility at the University of Texas Southwestern Medical Center at Dallas. (Protocol # 2015-101064)

Wild animals: Study does not involve wild animals.

Reporting on sex: Sex was considered in study design. Animals were sexed by observation of external genitalia. All data in the manuscript has been reported disaggregated by sex. Sex based analysis were performed for all animal experiments.

Field-collected samples: Study does not involve samples collected from the field.

Ethics oversight	All experiments involving live animals were approved by IACUC of UT Southwestern Medical Center (Protocol # 2015-101064).

Note that full information on the approval of the study protocol must also be provided in the manuscript.

Plants

Seed stocks	N/A
Novel plant genotypes	N/A
Authentication	N/A